Report

Cell Reports

Physiological Plasticity of Neural-Crest-Derived Stem Cells in the Adult Mammalian Carotid Body

Graphical Abstract

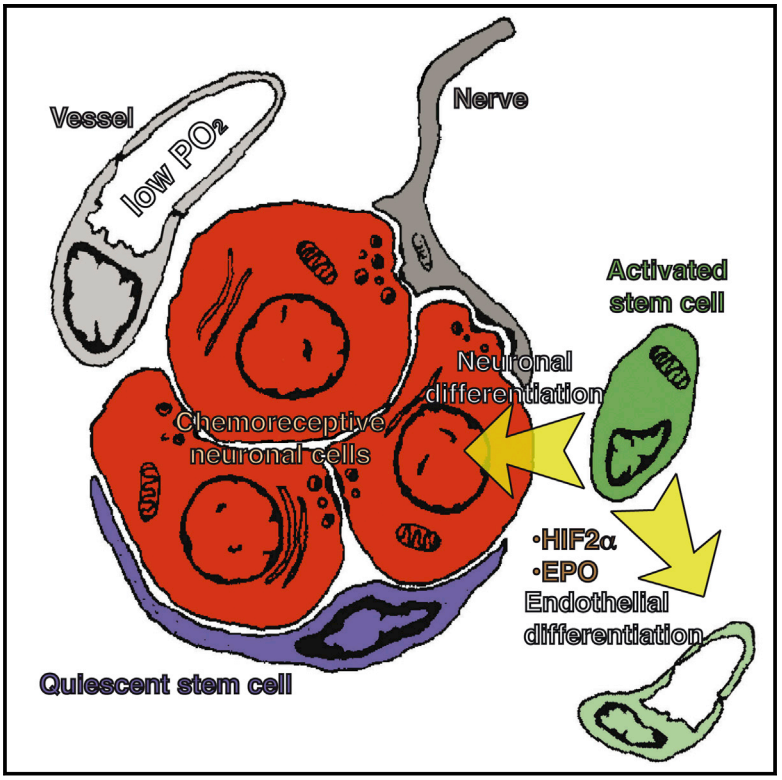

Highlights

- Adult carotid body stem cells display multipotency during organ adaptation to hypoxia
- Neural-crest-derived stem cells contribute to angiogenesis in the adult carotid body
- Endothelial differentiation from carotid body stem cells is HIF2α and EPO dependent

Authors

Valentina Annese,
Elena Navarro-Guerrero,
Ismael Rodríguez-Prieto, Ricardo Pardal

Correspondence

vannese@us.es (V.A.),
rpardal@us.es (R.P.)

In Brief

Annese et al. find that neural-crest-derived stem cells residing in the adult carotid body are multipotent. These cells have the capacity to contribute to both neurogenesis and angiogenesis during organ acclimatization to hypoxia. Endothelial fate specification is achieved by intrinsic (HIF2α) and extrinsic (EPO) mechanisms.

Annese et al., 2017, Cell Reports *19*, 471–478
April 18, 2017
http://dx.doi.org/10.1016/j.celrep.2017.03.065

Cell Reports
Report

Physiological Plasticity of Neural-Crest-Derived Stem Cells in the Adult Mammalian Carotid Body

Valentina Annese,[1,*] Elena Navarro-Guerrero,[1] Ismael Rodríguez-Prieto,[1] and Ricardo Pardal[1,2,*]
[1]Departamento de Fisiología Médica y Biofísica, Instituto de Biomedicina de Sevilla (IBiS), Hospital Universitario Virgen del Rocío/CSIC/Universidad de Sevilla, Seville 41013, Spain
[2]Lead Contact
*Correspondence: vannese@us.es (V.A.), rpardal@us.es (R.P.)
http://dx.doi.org/10.1016/j.celrep.2017.03.065

SUMMARY

Adult stem cell plasticity, or the ability of somatic stem cells to cross boundaries and differentiate into unrelated cell types, has been a matter of debate in the last decade. Neural-crest-derived stem cells (NCSCs) display a remarkable plasticity during development. Whether adult populations of NCSCs retain this plasticity is largely unknown. Herein, we describe that neural-crest-derived adult carotid body stem cells (CBSCs) are able to undergo endothelial differentiation in addition to their reported role in neurogenesis, contributing to both neurogenic and angiogenic processes taking place in the organ during acclimatization to hypoxia. Moreover, CBSC conversion into vascular cell types is hypoxia inducible factor (HIF) dependent and sensitive to hypoxia-released vascular cytokines such as erythropoietin. Our data highlight a remarkable physiological plasticity in an adult population of tissue-specific stem cells and could have impact on the use of these cells for cell therapy.

INTRODUCTION

The carotid body (CB), a neural-crest-derived paired organ located in the carotid bifurcation, is the main arterial chemoreceptor in mammals and facilitates reflex hyperventilation during hypoxia (López-Barneo et al., 2001). In addition, the CB is able to undergo neurogenesis to contribute to acclimatization of the organism during a persistent hypoxia (Edwards et al., 1971; Arias-Stella and Valcarcel, 1976; Heath et al., 1982; Wang and Bisgard, 2002). We have previously shown that glia-like sustentacular, or type II, cells surrounding chemosensory neuron-like glomus cells are neural crest stem cells (NCSCs) and contribute to CB growth in hypoxia by differentiating into new glomus cells (Pardal et al., 2007; Platero-Luengo et al., 2014). In addition to this neurogenic activity, a profound angiogenic process takes place in the hypoxic CB (Wang and Bisgard, 2002; Chen et al., 2007a). Whether neural-crest-derived adult CB stem cells (CBSCs) are able to differentiate into vascular cells, contributing to angiogenesis in vivo, in addition to neurogenesis, is largely unknown. We have recently described the presence of mesectoderm-restricted progenitors within CB parenchyma and have shown that these cells are able to convert into endothelial cells in vitro (Navarro-Guerrero et al., 2016). Therefore, the CB constitutes an ideal model where to study the potential plasticity of an adult population of NCSCs.

Utilizing both in vitro assays and in vivo cell-fate mapping experiments, we show that adult CBSCs do indeed retain multipotent differentiation capacity, being able to convert into endothelial cells (ECs) contributing to hypoxia-induced angiogenesis during acclimatization of the organ. Moreover, we provide mechanistic insight into this process by showing that CBSCs differentiate into ECs via a hypoxia inducible factor (HIF)-dependent mechanism and in response to hypoxia-released molecules such as erythropoietin. Thus, CBSCs use plasticity to facilitate physiological adaptation of the CB, and hence the organism, to hypoxia.

RESULTS

CBSCs Differentiate Into Vascular Cell Types under Hypoxic Conditions

In order to test the ability of CBSCs to contribute to vascular cell types, we decided to perform in vivo cell-fate mapping using *GFAP-cre/floxed LacZ* or *YFP* transgenic mice. These animals express the β-galactosidase enzyme (β-gal), or the yellow fluorescent protein (YFP), in GFAP$^+$ CBSCs and their derivatives (Pardal et al., 2007). However, the human GFAP promoter in this type of construct is not expressed in all GFAP$^+$ mouse cells, as previously revealed in brain astrocytes (Malatesta et al., 2003). In the case of CB, a first exposure to hypoxia (7 days; Figure S1) needs to be performed in order to activate the construct (Pardal et al., 2007), and only around 50% of GFAP$^+$ CBSCs get labeled (Figure S1F). After this first exposure to hypoxia, only GFAP$^+$ CB stem cells and their derivatives in resting conditions, i.e., some nestin$^+$ progenitor cells, appear labeled (Figures S1G and S1H), confirming the specificity of the construct. After construct activation, we exposed *GFAP-cre/floxed LacZ* mice to hypoxia for 7 days (for hypoxic stimulus confirmation, see Figures 4K and S5C) and interrogated vascular cells for the expression of *LacZ*. By using an antibody against β-gal, and GSA I, an endothelium-specific lectin, we found that 16.3% ± 2.7% of ECs were positive for β-gal (39 out of 229 GSA I$^+$ cells analyzed; Figures 1A and S1J). No single β-gal$^+$ GSA I$^+$ cell was found in the

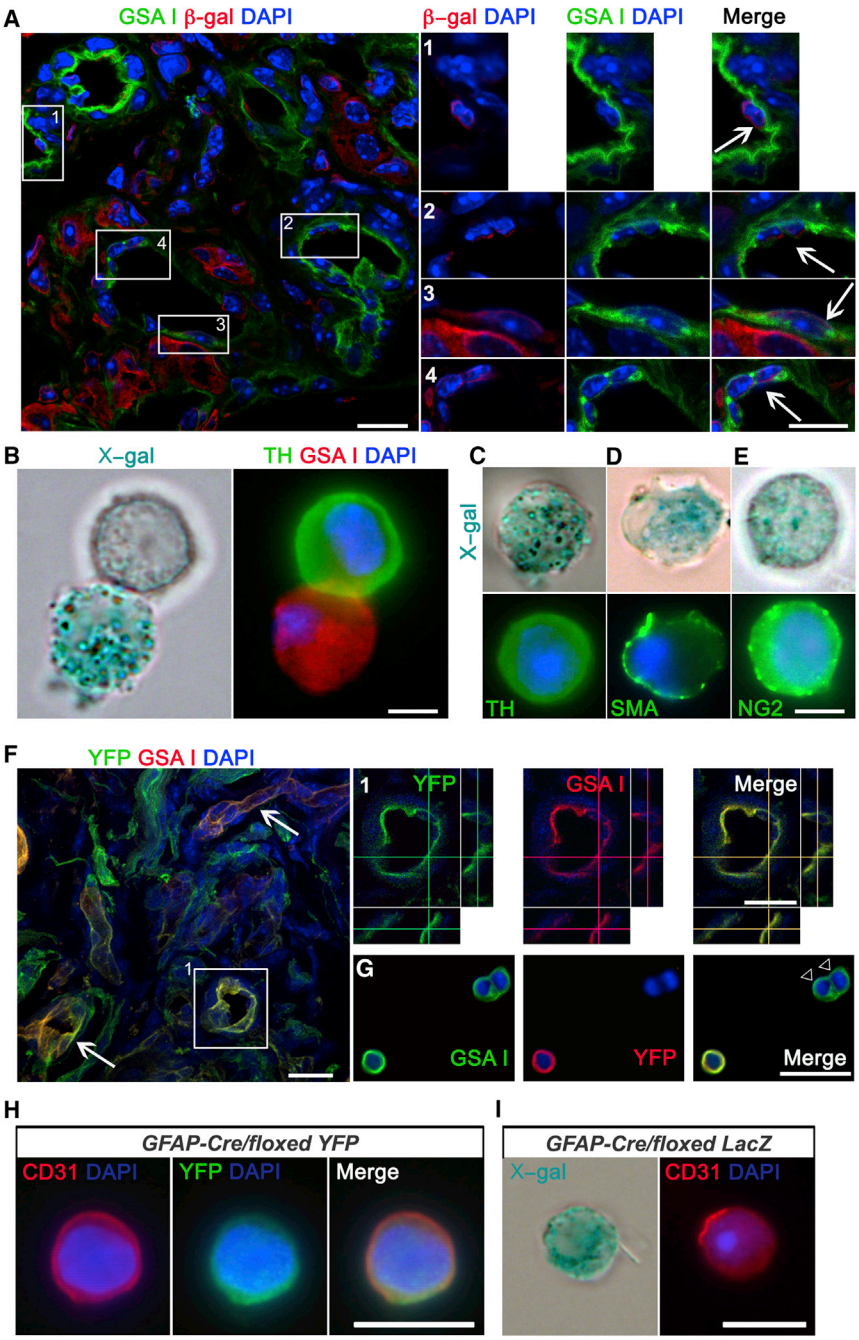

Figure 1. CB Stem Cells Contribute to Angiogenesis in Addition to Neurogenesis under Hypoxia

(A) Z stack projection picture obtained by confocal microscopy from a CB section of a hypoxic *GFAP-cre/floxed LacZ* mouse, immunostained with an antibody against β-galactosidase (red) and stained with the endothelial marker GSA I (green). ECs derived from GFAP$^+$ type II cells are shown in the enlargements of the boxed areas (arrows). Scale bars, 10 μm. Confocal pictures were taken in sections from two animals per group.

(B–E) Examples of X-gal$^+$ cells dispersed from the CB of hypoxic *GFAP-cre/floxed LacZ* mice. The pictures illustrate the appearance of X-gal$^+$ ECs (GSA I$^+$, B), glomus cells (TH$^+$, C), smooth muscle cells (SMA$^+$, D), and pericytes (NG2$^+$, E). Scale bars, 5 μm. n = 3 independent experiments.

(F) Fluorescence confocal microscopy pictures of CB sections from hypoxic *GFAP-cre/floxed YFP* mouse stained with anti-YFP antibody (green) and rodhamine-conjugated GSA I lectin. Arrows point to double-positive vessels. A higher magnification of the boxed region depicted in (F), showing z axis projection views, is shown in (1). Scale bars, 25 μm. n = 3 animals per experimental group.

(G) Picture of ex vivo hypoxic CB preparation stained with GSA I (green) and immunolabeled with an antibody against YFP reporter protein (red). Note the presence of GSA I positive ECs, negative for the reporter protein (white arrowheads). Scale bar, 25 μm.

(H and I) Examples of GFAP$^+$ cell-derived CD31$^+$ ECs, found in CB cell dispersions from both *GFAP-cre/floxed YFP* (H) and *GFAP-cre/floxed LacZ* (I) mice. Scale bars, 20 μm.

See also Figures S1 and S2.

CBs of normoxic *GFAP-cre/floxed LacZ* littermate mice (99 GSA I$^+$ cells analyzed), a result that was confirmed with YFP transgenic mice (Figure S1D). Differentiation of GFAP$^+$ CBSCs into ECs was confirmed in CB dispersed cells from hypoxic *GFAP-cre/floxed LacZ* mice, by using classical X-gal staining to reveal the activity of β-gal, and fluorescent cytochemistry to detect GSA I (Figure 1B), or the endothelial markers CD31 (Figure 1I), or von Willebrand factor (vWF; Figures S1K and S1L). Moreover, by using this CB ex vivo preparation, we confirmed neuronal differentiation capacity of GFAP$^+$ CBSCs in the same mice (Figure 1C). Interestingly, by using a smooth muscle cell marker (SMA; Figure 1D) and a pericyte marker (NG2; Figure 1E), we also uncovered the ability of CB neural progenitors to convert into other mesenchymal cell types forming the vascular compartment, suggesting that CB progenitors can give rise to complete blood vessels. The use of a second type of reporter mouse strain (*GFAP-cre/floxed YFP* mice) corroborated the cell-fate mapping results, both at the immunochemical (Figures 1F–1H) and flow cytometry (fluorescence-activated cell sorting [FACS]; Figure S1I) levels. The percentage of YFP$^+$ GSA I$^+$ cells, obtained from *GFAP-cre/floxed YFP* mouse CBs, was smaller (9.31% ± 0.59%) than from the *LacZ* mouse model, probably due to differences in Cre-mediated excision efficiencies between the two reporter genes used. The use of a different EC marker, such as CD31, for cell-fate mapping (Figures 1H, 1I, and S1I) yielded qualitatively very similar results. No single EC, labeled with the reporter gene, was found when analyzing the CB of *TH-Cre/floxed LacZ* mice (Figure S1M), ruling out an unspecific

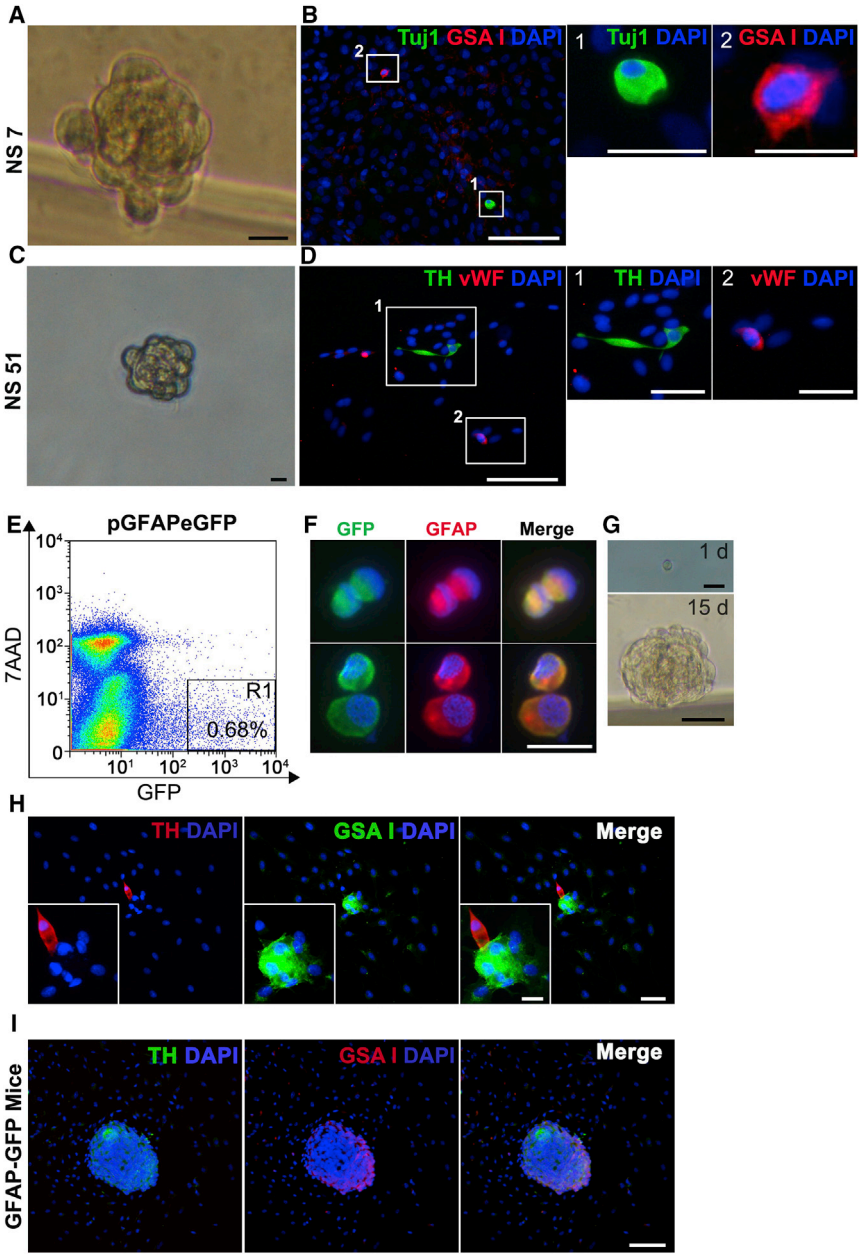

Figure 2. Single Progenitor Cells Display Multipotency In Vitro

(A and C) Bright-field photographs of secondary NS formed from single progenitors derived from enzymatic dispersion of primary NS. Scale bars, 5 μm.

(B and D) Immunofluorescence pictures of adherent secondary NS obtained from a single NS-derived progenitor cell (NSPC). Combinations of different cellular markers were tested inside the same colony (Tuj1 [green] and GSA I [red] in B, and TH [green] and vWF [red] in D). Scale bars, 100 μm. B1 and B2 and D1 and D2 show high-magnification images of the areas boxed in (B) and (D). Scale bars, 10 μm, in B1 and B2, and 30 μm, in D1 and D2. n = 4 primary NS cultures.

(E) Flow cytometry plot of dispersed rat CB cells transfected with *pGFAP-eGFP* plasmid.

(F) Image representing GFAP$^+$ cell enrichment in GFP$^+$ cell population sorted out by flow cytometry. Scale bar, 10 μm.

(G) Bright-field pictures showing the ability of single-cell plated GFP$^+$ cells (1 d) to form NS after 15 days (15 d) in culture. Scale bars, upper panel 10 μm and bottom panel 50 μm.

(H) Example of a single-cell-derived NS, containing cells of both neuronal (TH, red) and endothelial (GSA I, green) lineages. Scale bars, 10 μm, in (H), and 5 μm, in inset.

(I) Single-cell plating experiment performed using dispersed CB cells from *hGFAP-GFP* mice. Picture shows an example NS, double positive for neuronal (TH, green) and endothelial (GSA I, red) markers. Scale bar, 50 μm.

See also Figure S3.

expression of Cre recombinase by ECs, and confirming the differentiation of GFAP$^+$ CBSCs into vascular cells.

We corroborated the multipotent differentiation capacity of CBSCs in vivo, by performing bluo-gal staining and electron microscopy (EM) on the CB of hypoxic *GFAP-cre/floxed LacZ* mice (see Figure S2 and its legend). Altogether, in vivo cell-fate mapping experiments identify CBSCs as multipotent neural-crest-derived adult stem cells contributing to both neurogenesis and angiogenesis during hypoxic acclimatization of the organ.

Single CBSCs Display Multipotentiality In Vitro

To directly prove the multipotential capacity of CBSCs to differentiate into both neuronal and vascular cell types, we performed single-cell deposition experiments in vitro (Figure 2). Out of 1,536 dispersed primary neurosphere (NS) cells plated, 200 of them gave rise to secondary NS. Upon plating onto adherent conditions, 15 of those NS (7.5%) contained both neuronal and mesectodermal cells within the colony (Figures 2A–2D and S3A–S3F), confirming differentiation into both cell lineages from a single progenitor cell. The percentage of multipotent progenitor cells is likely being underestimated due to the lack of appropriate neuronal differentiation conditions in the single-cell plating assay. In addition to Tuj1 and GSA I markers (Figure 2B), we have corroborated the presence of neuronal and mesectodermal cells with different widely used markers: tyrosine hydroxylase (TH) for dopaminergic neuronal cells and vWF, NG2, and CD34 for vascular cells (Figures 2D and S3). We also performed single-cell plating analysis with FACS-sorted rat CB cells previously transfected with a *pGFAP-eGFP* construct, where 100% of GFP$^+$-sorted cells were GFAP$^+$ CBSCs (Figures 2E and 2F). Although the frequencies of NS formation and neuronal differentiation were quite low, likely due to transfection- and FACS-induced damage, and lack of optimal neuronal differentiation conditions, we were able to find some examples of

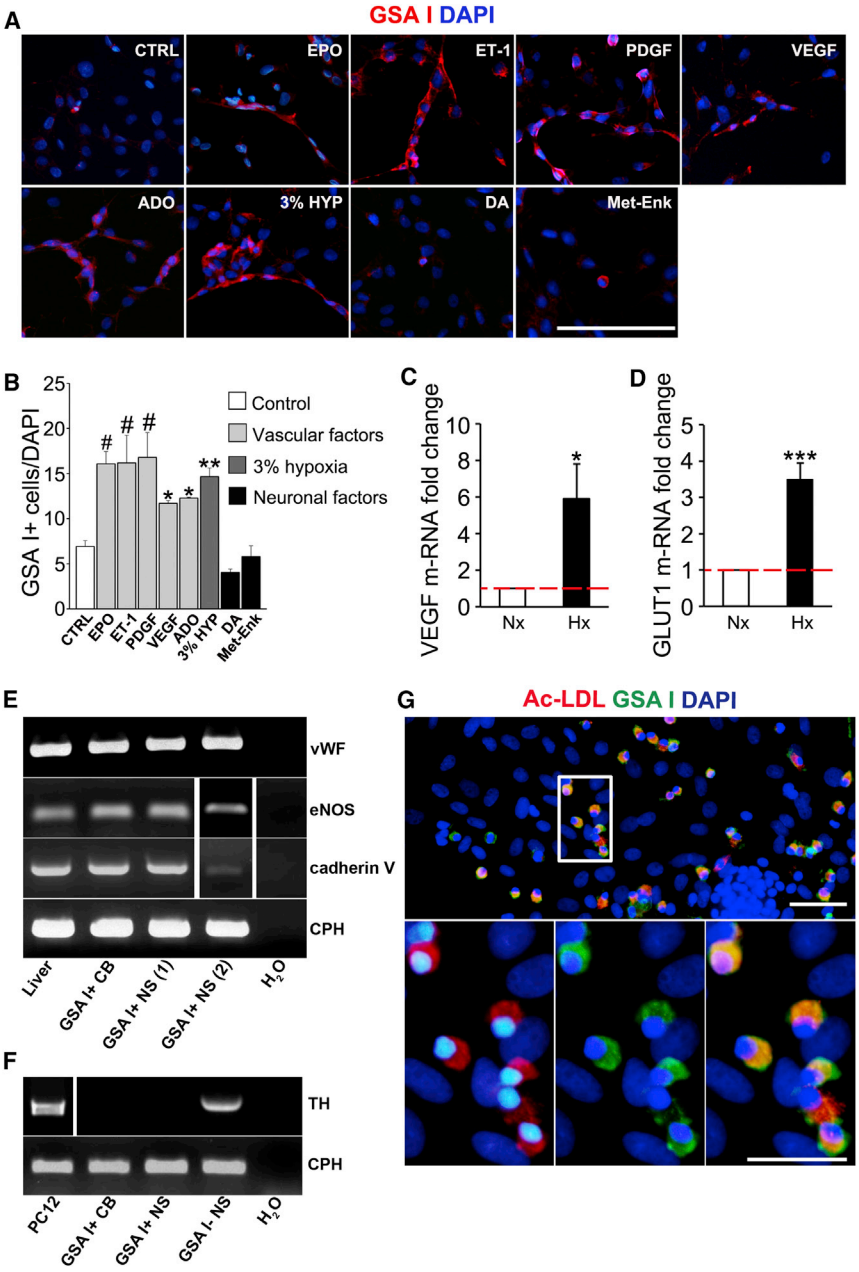

Figure 3. Vascular Factors Increase CBSC Endothelial Differentiation In Vitro

(A) Epifluorescent detection of GSA I (ECs; red) in adherent NS cultured on fibronectin in standard neural crest culture medium without mitogens (CTRL) and supplemented with vascular or neuronal factors. Scale bar, 200 μm.

(B) Quantification graph indicating the mean percentage of GSA I$^+$ cells among total cells in different culture conditions. Data are represented as the mean ± SEM.; *p ≤ 0.05, **p ≤ 0.01; # p ≤ 0.001, one-way ANOVA Newman-Keuls post hoc test compared to CTRL measurement. n = from three to nine independent NS cultures.

(C and D) Graphs representing a significant increase in mRNA expression of two classical hypoxia-inducible genes, VEGF (C) and GLUT1 (D). n = 4 independent NS cultures. In vitro hypoxia experiments were performed at 3% O_2. Data are represented as mean ± SEM.

(E) RT-PCRs revealing expression of mature endothelial markers in rat liver and in GSA I$^+$ cells isolated from CB or adherent NS by flow cytometry.

(F) Agarose gel showing TH mRNA amplified by RT-PCR in GSA - cell fraction isolated from adherent NS. Three independent RNA extractions were tested for each gene expression analysis.

(G) Binding of FITC-GSA I and uptake of Dil-acetylated LDL (Ac-LDL) in ECs in vitro, visualized by fluorescence microscopy. Nuclei are counterstained with DAPI (blue). Scale bars, 50 μm (top) and 25 μm (bottom). n = 3 NS cultures.

See also Figures S3, S4, and S6.

multipotent differentiation from single CBSCs (Figures 2G and 2H). Consistently, we also found multipotent differentiation when plating single GFP$^+$ cells from CBs of *GFAP-eGFP* transgenic mice (Figure 2I). Altogether, our single-cell plating data confirm multipotent differentiation capacity in CBSCs.

CBSCs Are Sensitive to Vascular Factors and Differentiate into Functional ECs

We next decided to explore the mechanisms by which CBSCs differentiate into ECs by using in vitro assays and rat CB cells, since the organ in rats is more manageable than in mice and the cells grow better in culture. Rat CBSC-derived NS can be plated onto adherent conditions where, upon mitogen withdrawal, cells are induced to differentiate. Using this assay, we found that CB progenitors differentiate into ECs (GSA I$^+$) when exposed to adherent substrate (control in Figures 3A and 3B). However, this differentiation was dramatically enhanced when the cells were exposed to hypoxia (see Figures 3C and 3D for hypoxia confirmation in vitro) or vascular factors (Figures 3A and 3B), such as erythropoietin (EPO), endothelin-1 (ET-1), platelet-derived growth factor (PDGF), vascular endothelial growth factor (VEGF), or adenosine (ADO). This differentiation effect appeared to be specific for vascular factors since the addition of typical CB neuronal factors, such as dopamine (DA) or methionine-enkephalin (Met-Enk) (González-Guerrero et al., 1993; Gauda and Gerfen, 1996), did not increase endothelial differentiation (Figures 3A and 3B). Interestingly, most vascular factors studied are consistently expressed in CB ECs, as assessed by RT-PCR on FACS-sorted CB cells (Figure S3H).

We next evaluated the expression of mature EC markers in GSA I$^+$ NS cells, using GSA I$^+$ CB dispersed cells and liver cells as positive controls (Figure 3E). We confirmed the expression of vWF, endothelial NO synthase (eNOS), and cadherin V, all of

them specific for mature endothelium. We also confirmed the expression of the receptors for the different vascular factors that activate endothelial differentiation in CBSCs (Figure S3I). Both CB- and NS-derived GSA I^+ cells lack expression of the receptor for DA (DRD2; Figure S3J), a neurotransmitter that did not increase endothelial differentiation (Figures 3A and 3B). As a control, we tested the expression of a CB neuronal marker (TH; Figure 3F), corroborating the lack of neuronal cell contamination in GSA I^+ populations. Moreover, we studied the functionality of CBSC-derived ECs obtained in vitro, by performing a low-density lipoprotein (LDL) uptake assay (Voyta et al., 1984). Out of 216 GSA I^+ cells analyzed from three independent cultures, 95% ± 1.5% of them were also positive for DiI-conjugated Ac-LDL (Figure 3G), confirming the uptake and intracellular storage of lipoproteins, and hence the functionality of ECs differentiated from CBSCs in vitro. Finally, we decided to confirm the vasculogenic capacity of CB progenitor cells by using Matrigel and a subcutaneous vasculogenesis assay (see Figure S4). Taken together, in vitro and in vivo functional assays and endothelial marker expression analysis indicate that neural-crest-derived CBSCs are able to differentiate into mature and functional ECs, supporting their capacity to participate in CB angiogenesis.

Endothelial Differentiation from CBSCs Is HIF Dependent and Sensitive to EPO

Interestingly, in vitro differentiation assays indicate that CBSC conversion into ECs is directly favored by low oxygen (see Figure 3A). Therefore, we decided to check whether CBSCs were intrinsically sensitive to hypoxia, and whether prolyl hydroxylase (PHD)/HIF pathway had a role in the vascular differentiation process. Our data (see Figure S5) clearly establish an important, although partial, role for HIF2α in the endothelial differentiation process. In addition, we decided to further study the role of a relevant hypoxia-induced vascular cytokine, EPO. EPO is a hematopoietic factor, finely regulated by oxygen tension (Franke et al., 2013), that has been described to participate in angiogenesis (Heeschen et al., 2003). In vitro results described above show that EPO increases the number of ECs obtained from CBSCs (see Figures 3A and 3B), and this is achieved without affecting neuronal differentiation (Figures 4A and 4B). Moreover, EPO receptor (EPOR) is expressed by both NS- and CB-derived nestin$^+$-activated progenitors (Figure 4C), suggesting a direct role of this cytokine on CBSC fate determination. Therefore, we decided to further examine the role of EPO on CB angiogenesis both in vitro and in vivo. The addition to adherent NS cultures of an antibody against EPO, that sequesters the hematopoietic cytokine, completely abrogated the increase in endothelial differentiation (Figures 4D and 4E). AG490 is an inhibitor of EPOR-associated Janus kinase (Jak) 2 that has been described to block EPO intracellular signaling (Lester et al., 2005). Addition of AG490 to EPO-treated adherent NS provoked a significant decrease in the number of ECs obtained (Figures 4D and 4E). Thus, our results suggest a specific role for EPO in the induction of endothelial differentiation from CBSCs in vitro.

We then decided to corroborate that EPO was being endogenously produced in the CB (Lam et al., 2009). As assessed by RT-PCR, CB cells produce EPO especially in hypoxic conditions (Figure 4F). In order to test whether cell-released EPO was able to direct vascular differentiation from CB progenitors, we performed hypoxic co-cultures of NS progenitor cells and ECs (Figure 4G). For these co-culture experiments, we used a well-characterized human EC line (HUVEC), which produces EPO (Figure 4H). The presence of HUVECs in the surrounding wells increased the amount of functional ECs in CB NS, an effect that was abrogated after the addition of a blocking antibody against EPO (Figures 4I and 4J), further corroborating the role of EPO on CB progenitor endothelial differentiation in vitro.

Finally, we wanted to test whether EPO was having a relevant role in hypoxia-induced CB angiogenesis in vivo. To this end, we used *GFAP-cre/floxed LacZ* transgenic mice exposed to hypoxia. Systemic injection of EPO signaling blocker AG490 in these mice significantly attenuated the typical hypoxia-induced EPO-mediated hematocrit increase (Figure 4K), corroborating the systemic action of the inhibitor. CBSC-derived newly formed ECs are labeled by β-galactosidase expression and hence appear with blue precipitate after X-gal staining (Figure 4L). Quantification of X-gal$^+$ cells in dispersed CB of these AG490-treated hypoxic mice revealed a decrease in the number of GSA I^+ ECs derived from CBSCs (Figure 4M), confirming the importance of EPO release and EPO signaling in CBSC-dependent angiogenesis.

DISCUSSION

In the present study, we show that adult CBSCs display multipotent differentiation capacity, giving rise to both neural and non-neural derivatives during physiological acclimatization of CB to hypoxia. Our results show that around 10%–15% of total ECs, after a single exposure of the organ to chronic hypoxia, are derived from CBSCs, and this value is likely being underestimated due to inefficient expression of transgenic constructs (Figure S1). Considering that ECs are described to double their number in the organ in response to hypoxia (Chen et al., 2007a), we therefore estimate that around one every three or four newly formed ECs is CBSC derived.

The ability of NSCs to differentiate into ECs has been previously described only in some in vitro studies (Wurmser et al., 2004; Ii et al., 2009) or in the context of nervous system oncological disease (Ricci-Vitiani et al., 2010; Wang et al., 2010; Pezzolo et al., 2011; Cheng et al., 2013). However, to the best of our knowledge, no other example has been reported about adult neural progenitors participating in a physiological process of angiogenesis in vivo.

In addition to the direct effect of hypoxia (see the role of HIF2α in the Supplemental Information), conversion of CBSCs into ECs is also clearly enhanced by the exposition of cells to vascular factors, which are particularly released during hypoxia (Fandrey, 1995). Among these factors, EPO has been described to regulate CNS progenitor behavior (Shingo et al., 2001; Chen et al., 2007b) and has a clear role enhancing vasculogenesis (Bahlmann et al., 2004; Wang et al., 2004). Our results show that CB cells produce this vascular factor mainly during hypoxia, indicating that locally produced EPO might play a role in angiogenesis in the CB. This result is consistent with the described production of EPO by neuronal glomus cells in the organ (Lam et al., 2009). Moreover, we have recently described a role for CB neuronal cells on the

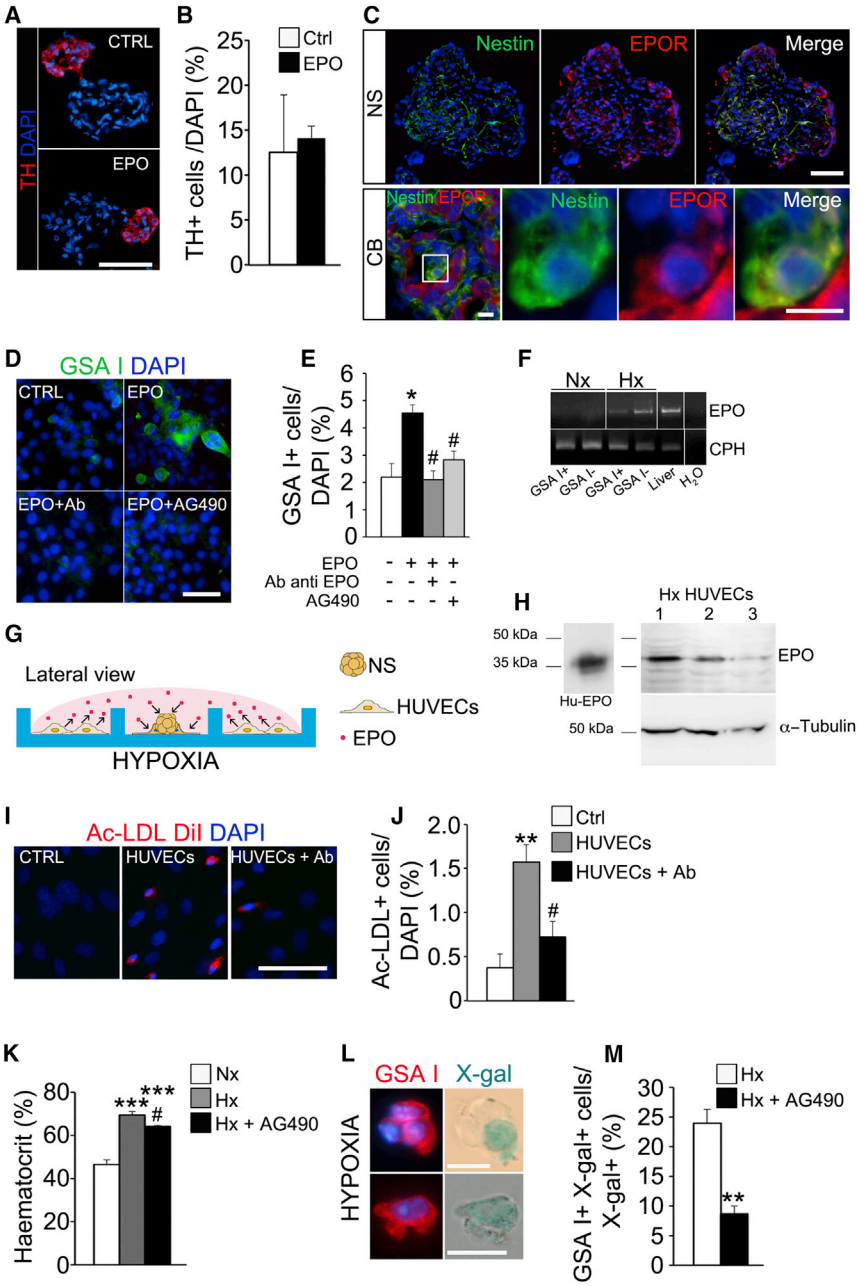

Figure 4. EPO Promotes the Endothelial Differentiation Capacity of CBSCs

(A) Immunohistochemistry pictures illustrating the size of TH$^+$ neuronal blebs in control and EPO-exposed NS. Scale bar, 50 μm.

(B) Quantification of the percentage of TH$^+$ cells versus total cells in NS sections, comparing control and EPO-treated NS. Data are represented as the mean ± SEM. No statistical differences were detected by Student's t test.

(C) Immunofluorescence pictures showing presence of EPO receptor (EPOR) on the surface of nestin$^+$ progenitors in both NS (upper panels) and CB (lower panels) tissues. Scale bars, 50 μm, in upper panels, and 10 μm, in lower panels.

(D) Images displaying EC differentiation within adherent cultures of primary NS in presence of EPO, EPO combined with EPO neutralizing antibody, or EPOR inhibitor (AG490). Scale bar, 50 μm.

(E) Quantification graph indicating the mean percentage of GSA I$^+$ cells in different culture conditions. Data are represented as the mean ± SEM; *p ≤ 0.05, one-way ANOVA Newman-Keuls post hoc test compared to control measurement (white bar), and #p ≤ 0.05, one-way ANOVA Newman-Keuls post hoc test compared to EPO treated measurement (black bar) (n = 3 cultures).

(F) Agarose gel showing the presence of EPO mRNA in hypoxic CB samples. n = 3.

(G) Schematic diagram describing the co-culture experiment.

(H) Representative western blot detecting EPO in three different hypoxic HUVEC protein extracts. The antibody recognizes in the cell extracts a band of about 38 kDa in concordance with human recombinant EPO (Hu-EPO).

(I) Pictures showing EC differentiation, detected by intracellular DiI-Ac-LDL uptake, occurring in NSPCs in different co-culture conditions. Parallel NS cultures without HUVECs served as control (CTRL). Scale bar, 25 μm.

(J) Quantification graph showing the percentage of DiI-Ac-LDL$^+$ cells detected in different co-culture conditions. Data are represented as the mean ± SEM.; **p ≤ 0.01, one-way ANOVA Newman-Keuls post hoc test compared to Ctrl measurement; #p ≤ 0.05, one-way ANOVA Newman-Keuls post hoc test compared to HUVEC co-culture measurement (n = 4 cultures).

(K) Histogram representing the significant increase of hematocrit, a typical hypoxia-sensitive EPO-mediated physiological variable, in experimental hypoxic animals (gray bar, n = 5) versus normoxic animals (white bar, n = 4). Consistently, treatment of hypoxic animals with EPOR inhibitor AG490 produced a significant decrease of hematocrit levels (black bar) when compared to hypoxia. In vivo experiments were carried out at 10% O_2. Data are represented as mean ± SEM.

(L) Representative microphotographs of X-gal$^+$ GSA I$^+$ cells observed in dispersed CB from *GFAP Cre/floxed LacZ* mice exposed to hypoxia for 7 days. Scale bars, 10 μm.

(M) Quantification of the percentage of X-gal$^+$ GSA I$^+$ cells versus total X-gal$^+$ cells found in dissociated CBs from *GFAP Cre/floxed LacZ* mice injected with vehicle (n = 3) or AG490 (n = 3), after 7 days of hypoxic treatment. **p ≤ 0.01, Student's t test compared to vehicle-treated hypoxic animals. Data are represented as mean ± SEM.

See also Figures S5 and S6.

proliferative activation of CBSCs through a different cytokine, ET-1 (Platero-Luengo et al., 2014). The additional release of EPO by CB glomus cells might represent another example of neuronal activity-dependent regulation of stem cell behavior, in this case promoting progenitors to participate in angiogenesis. Nevertheless, we cannot formally discard an additional role for circulating EPO in CB angiogenesis. Altogether, our results suggest that CBSCs retain mesectodermal differentiation potential,

resembling neural progenitors in the peripheral nervous system during development (Le Douarin et al., 2008). This ability allows them to participate in physiological angiogenesis, in addition to neurogenesis, during adaptation of the organ to hypoxia. This finding might be relevant to understand the pathophysiology of this chemoreceptor organ and to improve the therapeutic use of these stem cells.

EXPERIMENTAL PROCEDURES

Animals

Male and female transgenic mice (4–6 weeks old or 8–9 months old for dimethyloxalylglycine [DMOG] in vivo experiments) and Wistar rats (6 weeks old) were housed and treated according to the animal care guidelines of the European Community Council (86/609/EEC). All experimental procedures were approved by the Committee on Animal Research at the University of Seville. Details about the hypoxic treatment and drug administration are given in the Supplemental Information.

Dissociation of CB Cells and NS Cultures

Rat and transgenic mouse CBs were dissociated by enzymatic treatment and cultured to form NS, following protocols previously described (Pardal et al., 2007). Specific details are given in the Supplemental Information.

Immunocytochemistry and Immunohistochemistry

Immunostainings were performed following standard procedures described elsewhere (Pardal et al., 2007). Antibodies used are listed in Table S1. Specific details about the immunostaining protocols are given in the Supplemental Information.

X-Gal Staining

Dispersed CB cells from *GFAP-cre/floxed LacZ* and *TH-cre/floxed LacZ* mice were plated in ultralow binding Petri dishes and allowed to recover superficial epitopes, lost upon enzymatic dispersion, in an incubator overnight. After that, standard protocols for X-gal staining were applied, as previously described (Pardal et al., 2007). Once X-gal staining was performed, we processed the cells for antibody staining as indicated previously.

EM

Carotid bifurcations were embedded in gelatin (80–100 bloom; Panreac) supplemented with 2% glutaraldehyde (Electron Microscopy Sciences), and 50-μm-thick slices were cut on a vibratome (VT1000S; Leica Microsystems). CB vibratome sections were processed for bluo-gal staining. Specific details about this staining are given in the Supplemental Information.

In Vitro Multipotency Assay

Primary NS were collected in 15-mL conical tubes and centrifuged at 100 × *g* for 1 min. Following aspiration of supernatant, NS were dispersed by Accutase (Sigma), gently pipetting up and down during 10 min. After enzymatic treatment, 4 mL of medium was added to quench enzymes. Dissociated NS cells were centrifuged for 5 min at 300 × *g* at 4°C. Afterward, cells were resuspended and cultured at clonal density on an ultralow binding 96-well plate. Secondary NS were re-plated onto adherent conditions using fibronectin pre-treated plates, as described before. After 3 days in culture, adherent NS colonies were fixed in 4% paraformaldehyde (PFA) and processed for immunolabeling and GSA I staining (see above).

Endothelial Differentiation Assay

NS obtained from dispersed rat CBs were re-plated onto adherent conditions using 5 μg/mL fibronectin (Biomedical Technologies) pre-treated 24-well plates, at a density of 4 or 5 NS/well. Drug treatments are described in the Supplemental Information. After growing for 3 days in adherent conditions, flat NS colonies were fixed and stained with rodhamine or fluorescein-conjugated GSA I (see Immunocytochemistry section). ImageJ software (National Institute of Health) was used for cell number quantifications.

RT-PCR and Real-Time qPCR

Total RNA was extracted from GSA I positive and negative cell fractions from dispersed adherent NS or dispersed rat CBs, using a commercial kit (RNeasy MICRO kit; QIAGEN), following manufacturer's instructions. For retrotranscription, cDNA was synthesized with QuantiTec Reverse transcription kit (QIAGEN), as indicated by manufacturer's instructions. Primer sequences are reported in Table S2. Original gels for all PCRs are shown in Figure S6.

Flow Cytometry

All sorts and analysis were performed in a MoFlo three-laser flow cytometer (DAKO Cytomation) and a LSR Fortessa (BD Biosciences), respectively. Specific details about flow cytometry protocols are given in the Supplemental Experimental Procedures.

Western Blot

Whole-cell protein extracts were obtained from HUVEC cell line, cultured during 3 days in hypoxic conditions (3% O_2) in EC basal medium-2 (EBM-2, Lonza) for EPO protein detection. Specific details about the western blot protocol are given in the Supplemental Experimental Procedures.

Statistics

Analyses of significant differences between means were carried out using the unpaired or paired two-tailed Student's t test. Newman-Keuls post hoc or Tukey's multiple comparison tests were used whenever a significant difference between three or more sample means was revealed by a one-way ANOVA. Tukey or Newman-Keuls test was used depending upon whether or not additional power is required to detect significant differences between means. p values ≤ 0.05 were considered significant. More details about the statistical analysis are given in the Supplemental Information.

SUPPLEMENTAL INFORMATION

Supplemental Information includes Supplemental Experimental Procedures, six figures, and two tables and can be found with this article online at http://dx.doi.org/10.1016/j.celrep.2017.03.065.

AUTHOR CONTRIBUTIONS

R.P. and V.A. designed the experiments. V.A. conducted most of the experiments. E.N.-G. and I.R.-P. assisted V.A. with some of the experiments. R.P. and V.A. wrote the paper.

ACKNOWLEDGMENTS

We thank CITIUS and María José Castro for technical assistance. We thank Ángela Molina for help with PCRs, Professor Andreas Brech for his scientific advice, Juan Francisco Martín Rodríguez for help with Statistics, and José I. Piruat, José López Barneo, and David Cano for their valuable comments on the manuscript. This research was supported by European grants (ERC Starting Grant: CBSCs) and by Spanish Ministry of Economy and Competitiveness grant (SAF2013-48535-P and SAF2016-80412-P). V.A. was supported by a Juan de la Cierva fellowship from the Spanish Ministry of Economy and Competitiveness.

Received: September 30, 2016
Revised: February 21, 2017
Accepted: March 27, 2017
Published: April 18, 2017

REFERENCES

Arias-Stella, J., and Valcarcel, J. (1976). Chief cell hyperplasia in the human carotid body at high altitudes; physiologic and pathologic significance. Hum. Pathol. *7*, 361–373.

Bahlmann, F.H., De Groot, K., Spandau, J.M., Landry, A.L., Hertel, B., Duckert, T., Boehm, S.M., Menne, J., Haller, H., and Fliser, D. (2004). Erythropoietin regulates endothelial progenitor cells. Blood *103*, 921–926.

Chen, J., He, L., Liu, X., Dinger, B., Stensaas, L., and Fidone, S. (2007a). Effect of the endothelin receptor antagonist bosentan on chronic hypoxia-induced morphological and physiological changes in rat carotid body. Am. J. Physiol. Lung Cell. Mol. Physiol. *292*, L1257–L1262.

Chen, Z.Y., Asavaritikrai, P., Prchal, J.T., and Noguchi, C.T. (2007b). Endogenous erythropoietin signaling is required for normal neural progenitor cell proliferation. J. Biol. Chem. *282*, 25875–25883.

Cheng, L., Huang, Z., Zhou, W., Wu, Q., Donnola, S., Liu, J.K., Fang, X., Sloan, A.E., Mao, Y., Lathia, J.D., et al. (2013). Glioblastoma stem cells generate vascular pericytes to support vessel function and tumor growth. Cell *153*, 139–152.

Edwards, C., Heath, D., and Harris, P. (1971). The carotid body in emphysema and left ventricular hypertrophy. J. Pathol. *104*, 1–13.

Fandrey, J. (1995). Hypoxia-inducible gene expression. Respir. Physiol. *101*, 1–10.

Franke, K., Gassmann, M., and Wielockx, B. (2013). Erythrocytosis: The HIF pathway in control. Blood *122*, 1122–1128.

Gauda, E.B., and Gerfen, C.R. (1996). Expression and localization of enkephalin, substance P, and substance P receptor genes in the rat carotid body. Adv. Exp. Med. Biol. *410*, 313–318.

González-Guerrero, P.R., Rigual, R., and González, C. (1993). Opioid peptides in the rabbit carotid body: Identification and evidence for co-utilization and interactions with dopamine. J. Neurochem. *60*, 1762–1768.

Heath, D., Smith, P., and Jago, R. (1982). Hyperplasia of the carotid body. J. Pathol. *138*, 115–127.

Heeschen, C., Aicher, A., Lehmann, R., Fichtlscherer, S., Vasa, M., Urbich, C., Mildner-Rihm, C., Martin, H., Zeiher, A.M., and Dimmeler, S. (2003). Erythropoietin is a potent physiologic stimulus for endothelial progenitor cell mobilization. Blood *102*, 1340–1346.

Ii, M., Nishimura, H., Sekiguchi, H., Kamei, N., Yokoyama, A., Horii, M., and Asahara, T. (2009). Concurrent vasculogenesis and neurogenesis from adult neural stem cells. Circ. Res. *105*, 860–868.

Lam, S.Y., Tipoe, G.L., and Fung, M.L. (2009). Upregulation of erythropoietin and its receptor expression in the rat carotid body during chronic and intermittent hypoxia. Adv. Exp. Med. Biol. *648*, 207–214.

Le Douarin, N.M., Calloni, G.W., and Dupin, E. (2008). The stem cells of the neural crest. Cell Cycle *7*, 1013–1019.

Lester, R.D., Jo, M., Campana, W.M., and Gonias, S.L. (2005). Erythropoietin promotes MCF-7 breast cancer cell migration by an ERK/mitogen-activated protein kinase-dependent pathway and is primarily responsible for the increase in migration observed in hypoxia. J. Biol. Chem. *280*, 39273–39277.

López-Barneo, J., Pardal, R., and Ortega-Sáenz, P. (2001). Cellular mechanism of oxygen sensing. Annu. Rev. Physiol. *63*, 259–287.

Malatesta, P., Hack, M.A., Hartfuss, E., Kettenmann, H., Klinkert, W., Kirchhoff, F., and Götz, M. (2003). Neuronal or glial progeny: Regional differences in radial glia fate. Neuron *37*, 751–764.

Navarro-Guerrero, E., Platero-Luengo, A., Linares-Clemente, P., Cases, I., López-Barneo, J., and Pardal, R. (2016). Gene Expression Profiling Supports the Neural Crest Origin of Adult Rodent Carotid Body Stem Cells and Identifies CD10 as a Marker for Mesectoderm-Committed Progenitors. Stem Cells *34*, 1637–1650.

Pardal, R., Ortega-Sáenz, P., Durán, R., and López-Barneo, J. (2007). Glia-like stem cells sustain physiologic neurogenesis in the adult mammalian carotid body. Cell *131*, 364–377.

Pezzolo, A., Parodi, F., Marimpietri, D., Raffaghello, L., Cocco, C., Pistorio, A., Mosconi, M., Gambini, C., Cilli, M., Deaglio, S., et al. (2011). Oct-4+/Tenascin C+ neuroblastoma cells serve as progenitors of tumor-derived endothelial cells. Cell Res. *21*, 1470–1486.

Platero-Luengo, A., González-Granero, S., Durán, R., Díaz-Castro, B., Piruat, J.I., García-Verdugo, J.M., Pardal, R., and López-Barneo, J. (2014). An O2-sensitive glomus cell-stem cell synapse induces carotid body growth in chronic hypoxia. Cell *156*, 291–303.

Ricci-Vitiani, L., Pallini, R., Biffoni, M., Todaro, M., Invernici, G., Cenci, T., Maira, G., Parati, E.A., Stassi, G., Larocca, L.M., and De Maria, R. (2010). Tumour vascularization via endothelial differentiation of glioblastoma stem-like cells. Nature *468*, 824–828.

Shingo, T., Sorokan, S.T., Shimazaki, T., and Weiss, S. (2001). Erythropoietin regulates the in vitro and in vivo production of neuronal progenitors by mammalian forebrain neural stem cells. J. Neurosci. *21*, 9733–9743.

Voyta, J.C., Via, D.P., Butterfield, C.E., and Zetter, B.R. (1984). Identification and isolation of endothelial cells based on their increased uptake of acetylated-low density lipoprotein. J. Cell Biol. *99*, 2034–2040.

Wang, Z.Y., and Bisgard, G.E. (2002). Chronic hypoxia-induced morphological and neurochemical changes in the carotid body. Microsc. Res. Tech. *59*, 168–177.

Wang, L., Zhang, Z., Wang, Y., Zhang, R., and Chopp, M. (2004). Treatment of stroke with erythropoietin enhances neurogenesis and angiogenesis and improves neurological function in rats. Stroke *35*, 1732–1737.

Wang, R., Chadalavada, K., Wilshire, J., Kowalik, U., Hovinga, K.E., Geber, A., Fligelman, B., Leversha, M., Brennan, C., and Tabar, V. (2010). Glioblastoma stem-like cells give rise to tumour endothelium. Nature *468*, 829–833.

Wurmser, A.E., Nakashima, K., Summers, R.G., Toni, N., D'Amour, K.A., Lie, D.C., and Gage, F.H. (2004). Cell fusion-independent differentiation of neural stem cells to the endothelial lineage. Nature *430*, 350–356.

Cell Reports, Volume *19*

Supplemental Information

Physiological Plasticity of Neural-Crest-Derived Stem Cells in the Adult Mammalian Carotid Body

Valentina Annese, Elena Navarro-Guerrero, Ismael Rodríguez-Prieto, and Ricardo Pardal

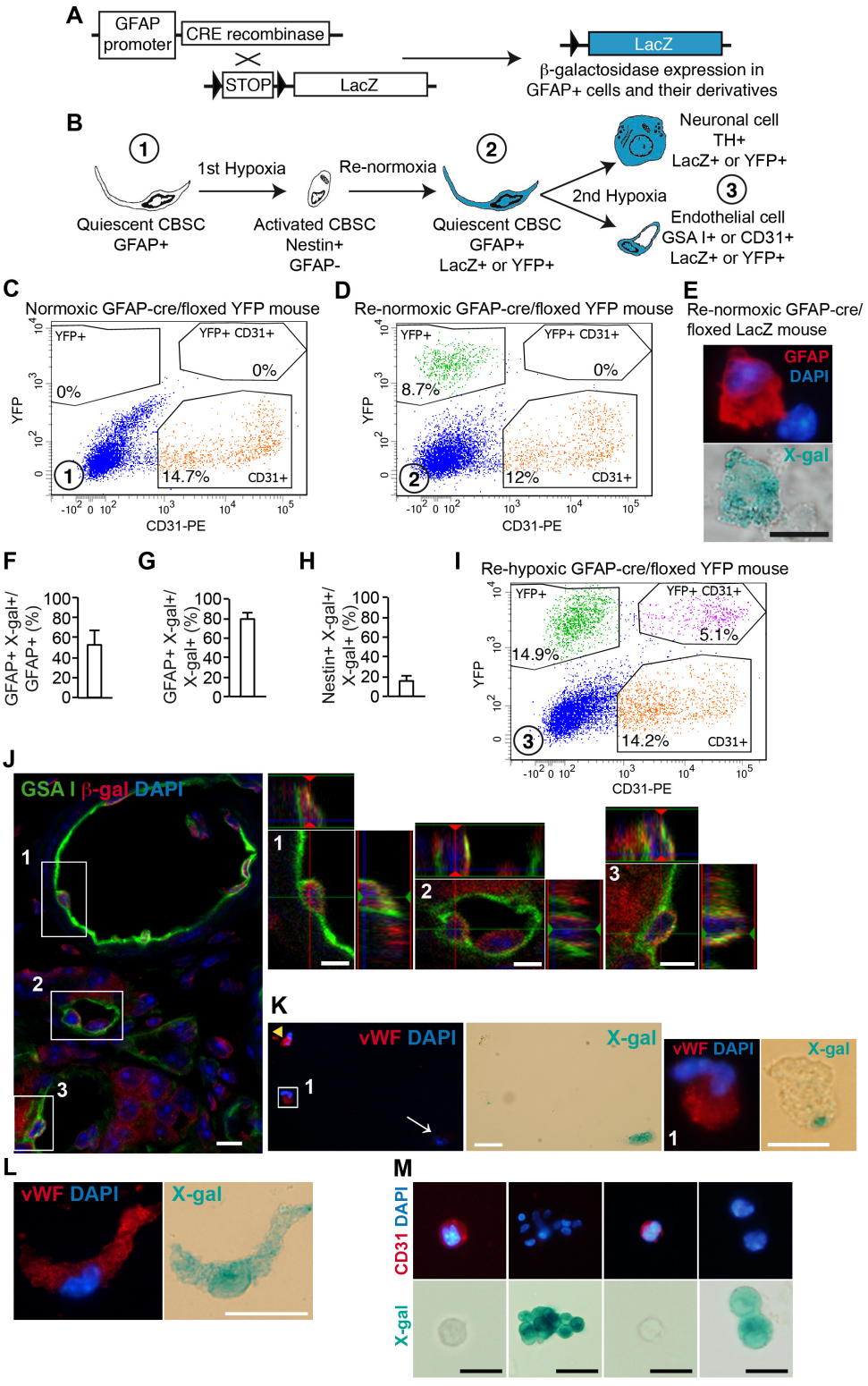

Figure S1. Cell fate mapping in the adult carotid body stem cell niche, Related to Figure 1.
(A) Diagram illustrating the CRE recombinase-mediated recombination event taking place in GFAP+ cells of *GFAP-Cre/floxed LacZ* mice to allow the expression of the reporter gene. Note that this recombination is irreversible, producing the labeling of all GFAP+ cell derivatives and hence enabling the cell fate mapping.
(B) Scheme of the cellular events taking place in the CB of *GFAP-Cre/floxed LacZ* or *YFP* mice during the first two expositions to hypoxia. The human origin of the GFAP promoter used in these transgenic animals makes the construct to behave as an inducible Cre, with the first exposure to hypoxia functioning

as the trigger stimulus to the expression of the recombinase.
(C) FACS plot showing CD31+ endothelial cells and YFP+ cells within the CB of *GFAP-Cre/floxed YFP* mice before the first exposure to hypoxia. Note the complete absence of recombined YFP+ cells.
(D) FACS plot showing CD31+ endothelial cells and YFP+ cells within the CB of a re-normoxic *GFAP-Cre/floxed YFP* mouse after the first exposure to hypoxia. Note the presence of YFP+ cells but without conversion into endothelial cells yet (absence of double positive cells).
(E) Fluorescent and bright field pictures of two CB dispersed cells from a re-normoxic *GFAP-Cre/floxed LacZ* mouse, illustrating the specific expression of the reporter enzyme in the GFAP+ cell. Scale: 10 μm.
(F) Quantification of GFAP/X-gal double positive cells among GFAP+ cells from dispersed CB of re-normoxic *GFAP-Cre/floxed LacZ* mice, illustrating that about half of GFAP+ cells get labeled after the first exposure to hypoxia. n=3 CB enzymatic cell dispersions (2 mice each cell dispersion).
(G, H) Quantification of GFAP+ (G) and Nestin+ (H) cells within X-gal+ cells in dispersed CB of re-normoxic *GFAP-Cre/floxed LacZ* mice, indicating that all labeled cells are GFAP+ stem cells with some basal activation of these cells to Nestin+ progenitors. n=3 CB enzymatic cell dispersions (2 mice each cell dispersion). No single CD31/X-gal double positive cell was found in these preparations, consistent with the results obtained by FACS (D).
(I) FACS plot showing YFP signal and CD31 staining in dispersed CB cells from *GFAP-Cre/floxed YFP* mouse after the second exposure to hypoxia. In this case, the presence of CD31/YFP double positive cells indicate that some labeled GFAP+ stem cells have undergone differentiation into endothelial cells.
(J) Confocal image of β-galactosidase (red) and GSA I (green) immunofluorescence performed on CB sections from *GFAP-Cre/floxed LacZ* mice. A higher magnification of the boxed regions depicted in (J), showing Z-axis projection views, is shown in (J1), (J2) and (J3). Scale bars: 5 μm.
(K, L) Examples of vWF+ endothelial cells derived from CBSCs (vWF+ X-gal+) and detected in dispersed CBs from hypoxic *GFAP-Cre/floxed LacZ* mice. (K1) Zoom of the boxed area in (K). Note in (K) the presence of a vWF+ endothelial cell not derived from CBSCs (yellow arrow head) and an unidentified X-gal+ cell (white arrow). Scale bars: 5 μm.
(M) Pictures showing the combination of CD31 immunolabeling with X-gal staining in dispersed CB cells from *TH-Cre/floxed LacZ* mice. No double positive cells were observed in any mice. n=3 CB enzymatic cell dispersions (2 mice each cell dispersion). Scale bars: 20 μm in the second column and 10 μm in the rest of columns.

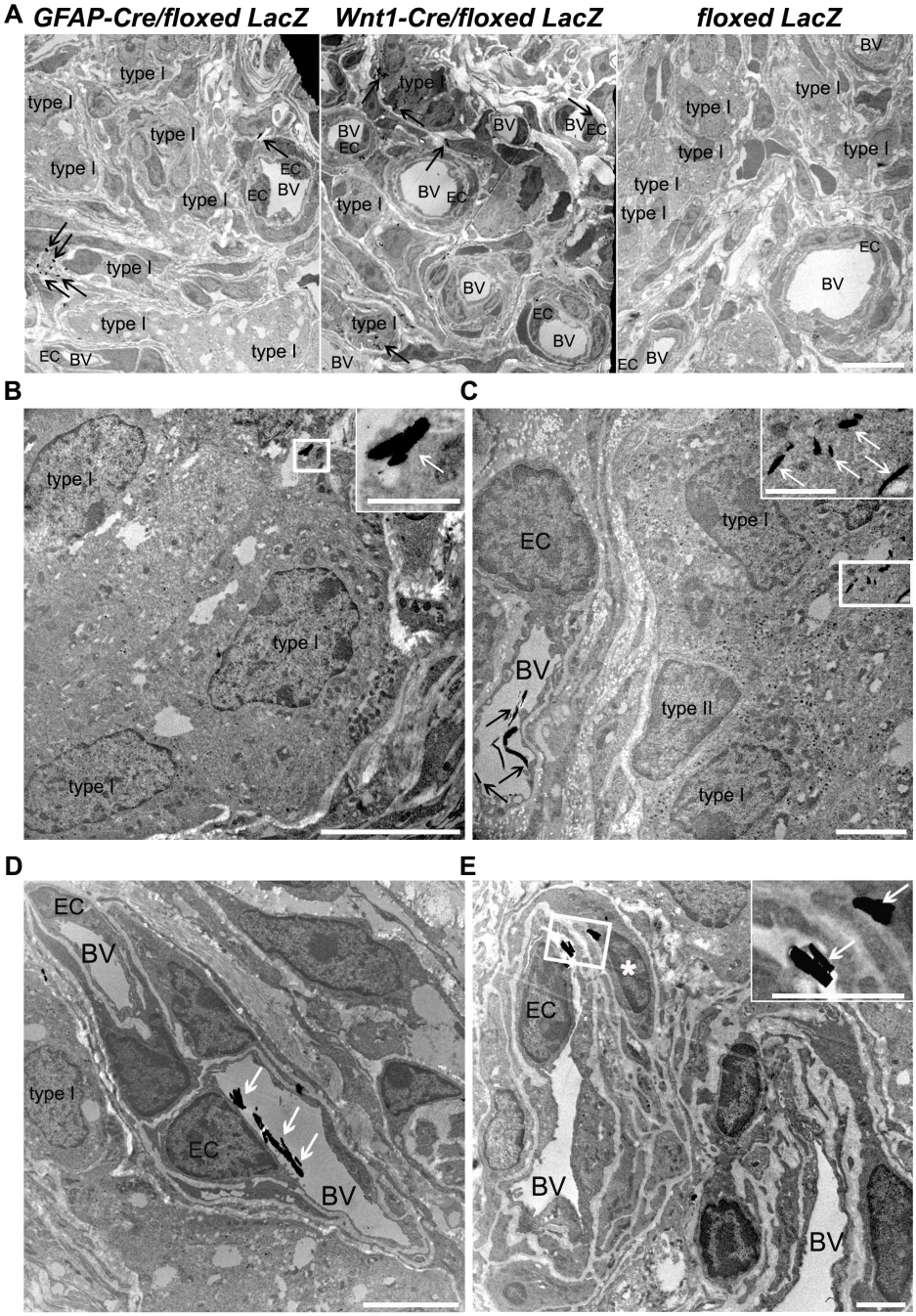

Figure S2. Electron microscopy corroborates GFAP+ progenitors giving rise to type I and endothelial cells in response to hypoxia, Related to Figure 1.

Bluo-gal is an alternative substrate for the β-gal enzyme, similar to X-gal, but the resulting electron dense precipitate is detectable by EM (Weis et al., 1991; Joseph et al., 2004).

(A) Low magnification electron micrographs of CB sections from *GFAP-cre/floxed LacZ*, *Wnt1-cre/floxed LacZ*, and control *floxed LacZ* mice. Dark arrows indicate Bluo-gal crystals in both *Wnt1-cre* and *GFAP-cre/floxed LacZ* strains. The level of bluo-gal staining in the CB of *GFAP-cre/floxed LacZ* mice was much lower than in the *Wnt1-cre/floxed LacZ* mice, consistent to what has been shown before for X-gal staining (Pardal et al., 2007). Note the total absence of Bluo-gal staining in the control *floxed LacZ* littermate mouse. Scale bar: 10 μm.

(B-E) Electronic micrographs of the CB of a *GFAP-Cre/floxed LacZ* mouse dissected and processed for Bluo-gal staining. Upon β-galactosidase action, Bluo-gal forms an electron-dense precipitate, visible as small black crystals (arrows) by electron microscopy. In addition to neuronal type I cells (B and C), recognized by the presence of dense-core vesicles, abundant mitochondria, and the typical condensation

of chromatin, we observed ECs, structurally identified at the wall of blood vessels, labeled with bluo-gal precipitates, which typically appeared in the vessel lumen (C-E). In some of these vessels, labeled cells with the typical shape of smooth muscle, surrounding the endothelium, could be observed (asterisk in (E)). No single bluo-gal positive cell was found in *floxed LacZ* control mice (A). Cellular plasma membrane appears light and fragmented due to the required fixation conditions, which provokes the diffusion of Bluo-gal precipitates out of the cells. Scale bars: 5 μm in (B) and (D); 2 μm in (C), (E) and inset in (E); 1 μm in insets in (B) and (C). n=3 animals.

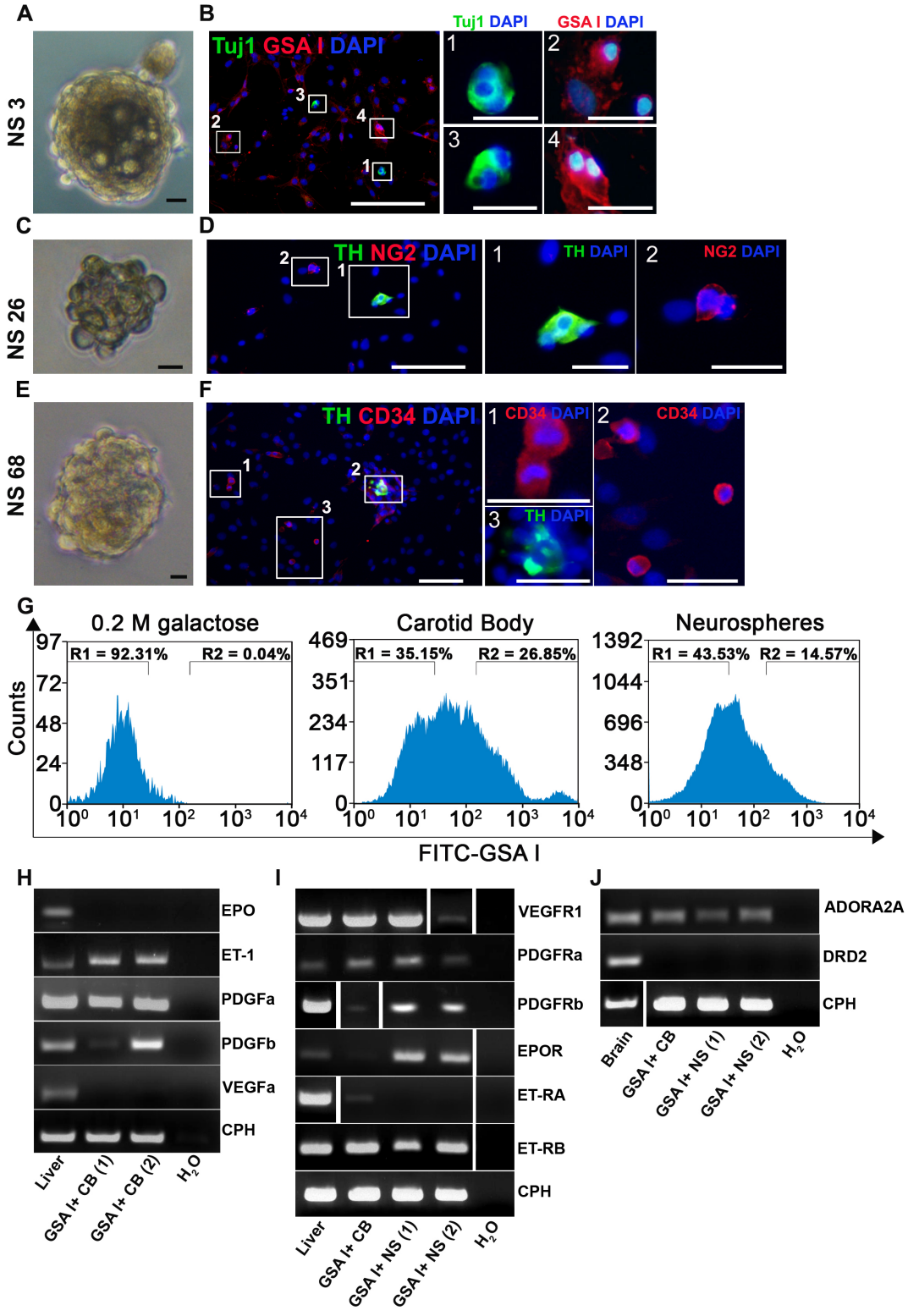

Figure S3. Single NS progenitor cells display multipotency *in vitro*, and CB GSA I+ endothelial cells are a source of vascular factors, Related to Figures 2 and 3.

(A, C, E) Bright field photographs of secondary neurospheres formed after 2 weeks in culture from single progenitors derived from enzymatic dispersion of primary neurospheres. Scale bars: 5 μm.

(B, D, F) Pictures showing the generation of both neuronal and mesectodermal cells within the colonies obtained from single neurosphere-derived progenitor cells (NSPC). Co-existence of different cellular markers was proved inside the same colony (Tuj1 (green) and GSA I (red) in (B), TH (green) and NG2 (red) in (D), and TH (green) and CD34 (red) in (F)). Scale bars: 100 μm. On the most right panels, high

magnification images of the areas boxed in (B), (D) and (F), are shown. Scale bars: 10 μm in (B1-4); 30 μm in (D1-2) and in (F1-2); and 50 μm in (F3). n=4 primary NS cultures.
(G) Analysis by flow cytometry of both rat CB and adherent neurosphere cells using GSA I lectin as an endothelial marker. A negative control using galactose is shown in the left panel.
(H) RT-PCR analysis in sorted GSA I+ cells (R2) from two different CBs, showing expression of vascular factors. Rat liver was used as positive control, and cyclophilin (CPH) was used as a loading control.
(I) RT- PCRs revealing expression of vascular factor receptors in rat liver and in GSA I+ cells isolated from CB or adherent neurospheres by flow cytometry. Loading control used was cyclophilin (CPH).
(J) RT-PCR displaying presence of ADORA2A mRNA in GSA I+ cells sorted from CB or adherent neurospheres by flow cytometry. DRD2 mRNA resulted below detection levels by RT-PCR (40 cycles) in GSA I+ cells obtained from both CB and neurospheres. Rat brain was used as positive control. Loading control was CPH. RNA expression for each gene was studied using 3 different RNA extractions obtained by cell sorter separation from 3 independent CB dispersions.

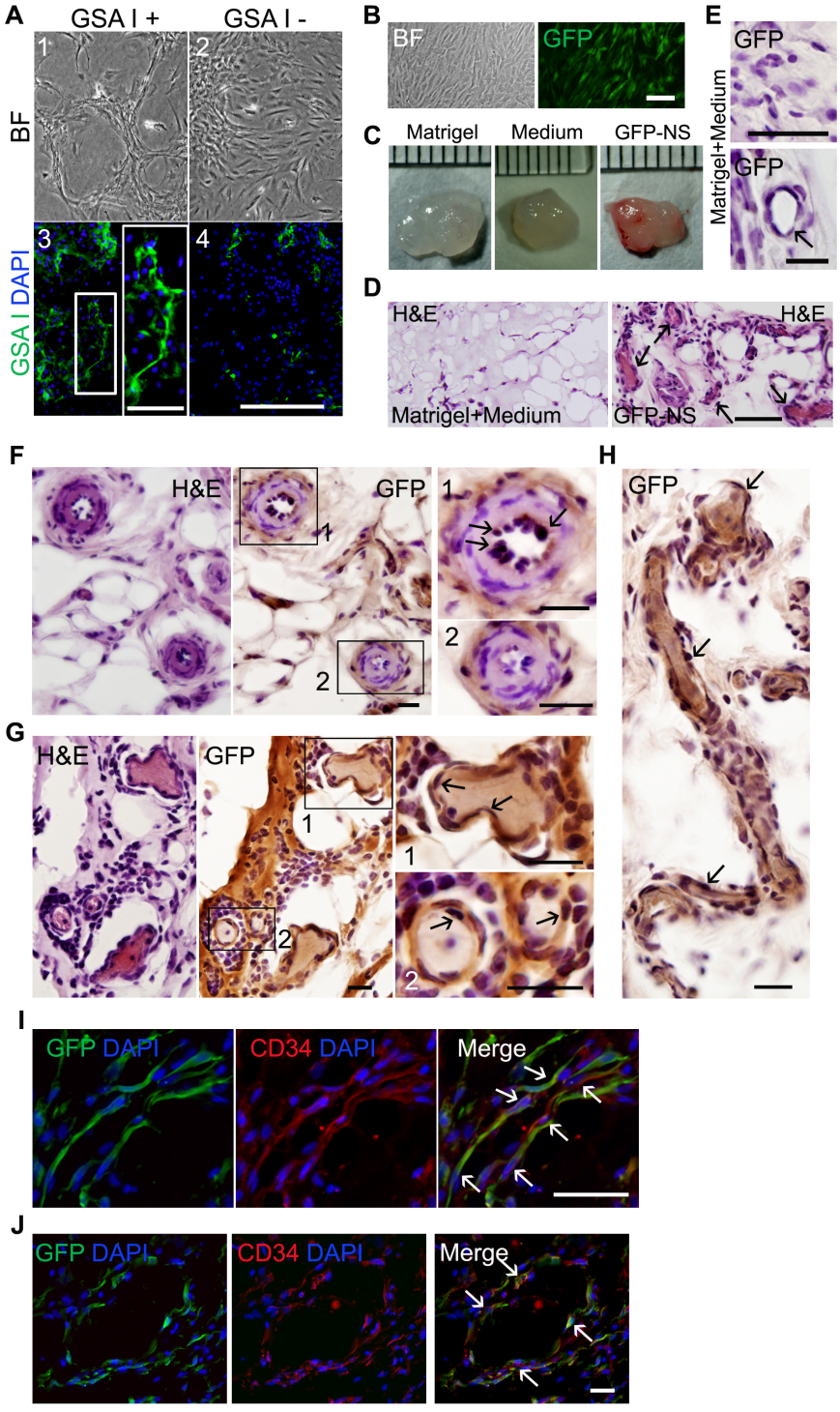

Figure S4. Vasculogenic potential of CBSC-derived NS cells, Related to Figure 3.
In order to test the vasculogenic potential of CB progenitor cells, we used NS cells, instead of FACS isolated CBSCs, due to the need for high cell numbers in these assays.
(A) Analysis by both phase contrast (1-2) and fluorescence (3-4) microscopy of the viability of an angiogenesis assay performed on matrigel coated plates (Benelli and Albini, 1999). Note how GSA I+ cells exhibit higher level of structural organization and a tendency to form multiple links between cells (1, 3) when compared to the GSA I negative cell fraction (2, 4). Scale bars: 500 μm, and 100 μm in the inset. n=3 independent experiments.
(B) Phase contrast (left panel) and fluorescence (right panel) representative photographs of NS cells infected with VSV-G pseudotyped lentiviral vector particles. Efficiency of infection was measured by GFP expression using fluorescence microscopy. Scale bar: 100 μm. n=3.

(C) Macroscopic view of matrigel plugs from an *in vivo* vasculogenesis assay, in which NS cells labeled with GFP (GFP-NS; panel B) were suspended in matrigel and injected subcutaneously in recipient animals (Melero-Martin et al., 2007), which are then exposed to hypoxia for one week. From left to right: matrigel plugs containing PBS alone, medium alone, and GFP-NS cells, harvested one week after implantation. Upon dissection of the transplants, reddish areas could be observed in NS cell-containing matrigels, but not in matrigel only or matrigel plus medium control transplants. Rulers are in mm.
(D) Hematoxilin/eosin (H&E) staining of implant thin sections containing medium alone (left) or GFP-NS cells (right). Note the presence of microvessels in the implant containing GFP-NS cells (arrows in the right panel), which were absent in control transplants. Scale bar: 100 μm.
(E) Bright field pictures of frozen sections of medium-containing matrigel plugs (negative control), subjected to immunostaining for GFP reporter protein. No GFP+ cells were detected, demonstrating the specificity of the antibody reaction. Few (arrow in the lower panel) or no vascular structures were observed in sections obtained from this type of negative control matrigel plugs. Scale bars: 50 μm in upper panel and 20 μm in lower panel.
(F, G) H&E and immunohistochemical staining with specific anti-GFP antibody of adjacent serial sections of matrigel plug containing GFP-NS cells one week after implantation, revealing that GFP-expressing NS cells contributed to the endothelial wall of blood-containing vessels (arrows in panels F1, G1, and G2). No GFP positive cells were found in sections from plugs with only medium (panel E). Some vessels completely negative for the GFP marker were also observed (panel F2), likely due to contribution of host-derived mesenchymal cells.
(H) Detail of a long vessel with numerous GFP immuno-positive cells in the wall (see arrows), confirming donor contribution to the assembled microvessels. Scale bars in (F), (G), and (H): 20 μm. n=3 transplanted rats.
(I, J) Fluorescent pictures showing blood vessels in NS cell-containing matrigel plugs, after 7 days of exposition to hypoxia. Detection of CD34 (red) and GFP (green) double positive endothelial cells (see arrows in merged pictures) confirmed NS cell-derived contribution to new vessel formation in matrigel plugs. Scale bars: 100 μm in (I) and 20 μm in (J).

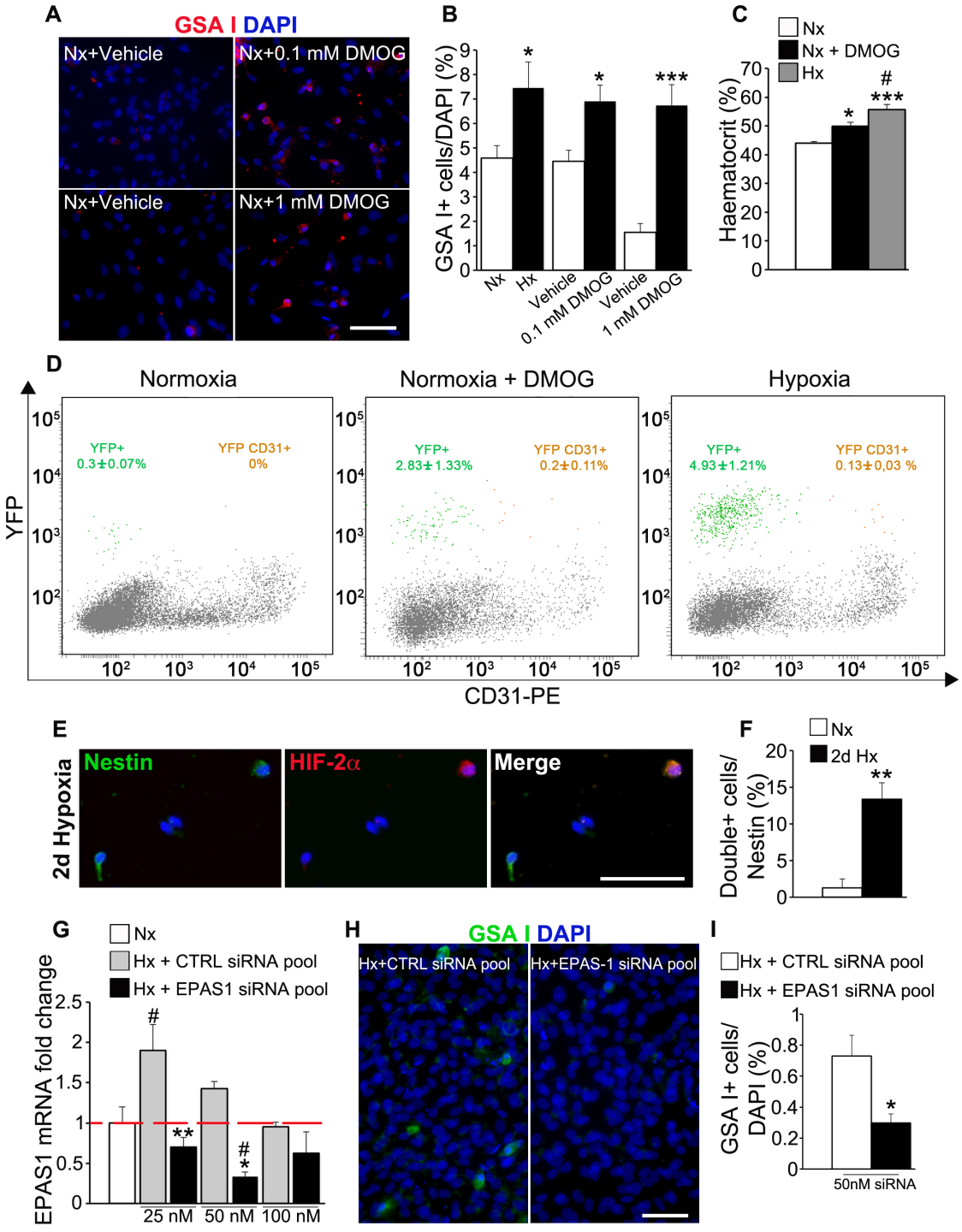

Figure S5. HIF-2α contributes to CBSC activation and endothelial differentiation, Related to Figure 4.
Inhibition of PHDs by lack of oxygen allows stabilization of HIFs, which in turn control the expression of a wide variety of hypoxia-sensitive genes (Kaelin and Ratcliffe, 2008).
(A) Immunofluorescent micrographs illustrating endothelial differentiation (GSA I+ cells in red) from NS cells cultured in adherent conditions on fibronectin, and in the presence of vehicle (left panel) or DMOG (right panel) in normoxic environment (Nx). Scale bar: 50 μm. Dimethyloxalylglycine (DMOG), elicited a similar increase in endothelial differentiation to that obtained by low oxygen (Figure 3A and B).
(B) Bar graph summarizing the percentage of GSA I+ cells (n=4 independent cultures) in adherent NS cells cultured under normoxia (Nx) or hypoxia (Hx), under normoxia in the presence of vehicle or 0.1 mM

DMOG, and under normoxia in the presence of vehicle or 1 mM DMOG. Data are represented as mean±s.e.m. *p≤0.05, ***p≤0.001, Student's t test comparing each treatment group (Hx, 0.1 mM DMOG, and 1 mM DMOG) to their respective control (Nx, and vehicles).
(C) Quantification of haematocrit in *GFAP-Cre/floxed YFP* mice exposed to hypoxia (10% O2, grey bar) or maintained in normoxic conditions and treated with DMOG (black bar), in comparison to normoxic untreated mice (white bar). Data is represented as mean±s.e.m.; One-Way ANOVA Tukey's multiple comparisons post hoc test compared to normoxia, *p≤0.05, ***p≤0.001, or compared to hypoxia, #p≤0.05 (n=6-7 mice). A clear but discrete increase in haematocrit was observed in DMOG-infused animals when compared to hypoxic animals.
(D) Cell fate mapping study performed by FACS analysis in dissociated CB cells from normoxic, normoxic plus injected DMOG (12 days), and hypoxic (12 days), *GFAP-Cre/floxed YFP* mice. Mean percentage values with standard errors for both YFP+ (green dots) and YFP+/CD31+ (orange dots) populations are reported in the plots. FACS plots are representative for 3 independent CB dispersions for each experimental group. Note how DMOG induced a clear increase in the number of YFP+ cells, including endothelial differentiation (CD31+), when compared to normoxic conditions, although the effect was more discrete than the one produced by hypoxia.
(E) Fluorescence micrographs illustrating stabilization of HIF-2α in activated progenitor cells (nestin+ and round) in hypoxic conditions. Rat CBSCs usually display cellular prolongations when they are quiescent, and become round and proliferative when activated (Pardal et al., 2007). The pictures show an example of a CBSC still with a cell prolongation, negative for HIF, and an activated round nestin+ CBSC, which clearly underwent HIF stabilization. Scale bar: 50 μm.
(F) Bar graph indicating the percentage of HIF-2α+ cells within nestin+ cell population, in both normoxic (white bar) and 2 days hypoxic CBs (black bar). The proportion of nestin+ progenitors that stabilize HIF, dramatically increases after only 2 days in hypoxic conditions (n=3 independent CB dispersions from 2 rats each). Data is represented as mean±s.e.m.; **p≤0.01, Student's t test compared to normoxic group.
(G) Specific inhibition of EPAS1 (the gene encoding for HIF2α) mRNA expression in dissociated NS cells transfected with different concentrations of EPAS1 siRNA pool (n=4 independent NS cultures). Data is represented as mean±s.e.m.; One-Way ANOVA Newman-Keuls multiple comparisons post hoc test compared to respective control (CTRL) pool concentration, *p≤0.05, **p≤0.01, or compared to normoxic conditions, #p≤0.05. Transfection with EPAS1 siRNA not only prevented hypoxia-induced increase in EPAS1 expression but also decreased EPAS1 basal expression when compared to normoxic conditions.
(H) Representative immunofluorescence pictures showing endothelial differentiation in enzymatically dispersed NS cells transfected with control siRNA pool (left panel) or EPAS1 siRNA pool, both under hypoxic conditions. Scale bar: 50 μm.
(I) Quantification of the percentage of GSA I+ cells differentiated from both CTRL-interfered (white bar) or EPAS1-interfered (black bar) NS cells in hypoxic conditions (n=3 independent NS cultures). Data is represented as mean±s.e.m.; *p≤0.05, Student's t test compared to Hx+CTRL siRNA pool group. Knocking-down HIF2α in NS progenitor cells clearly decreases the ability of these cells to convert into endothelial cells, clearly confirming an important role for PHD/HIF pathway in endothelial differentiation from CBSCs. These data demonstrate that CBSC differentiation into endothelial cells is directly sensitive to hypoxia, with a clear role of PHD/HIF system in the process. Therefore, hypoxia directly favors differentiation from CBSCs into both neuronal (Platero-Luengo et al., 2014) and endothelial lineages, being cell fate choice apparently more dependent on the presence of paracrine signaling. HIF factors include a number of different isoforms. HIF1α has been involved in neural crest proliferation and specification (Barriga et al., 2013), although it does not seem to play a role in CB growth (Platero-Luengo et al., 2014; Hodson et al., 2016). In contrast, HIF2 α has been recently described to have an important role in hypoxia acclimatization (Arsenault et al., 2013; Bishop et al., 2013), and more specifically in CB growth (Hodson et al., 2016). Our data confirm HIF2α as an important player in the induction of angiogenesis from CBSCs.

Related to Figure 3E

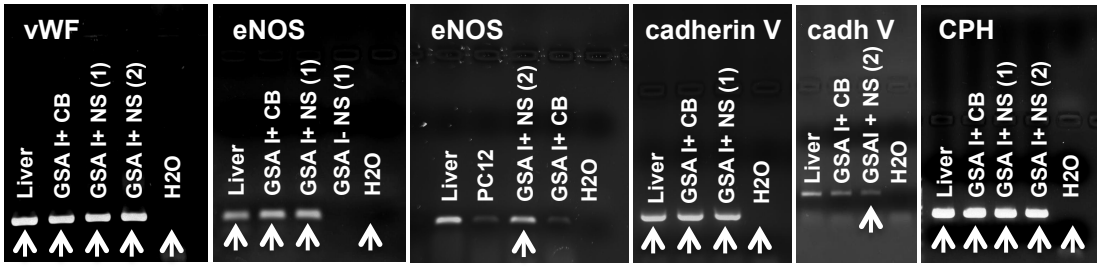

Related to Figure 3F

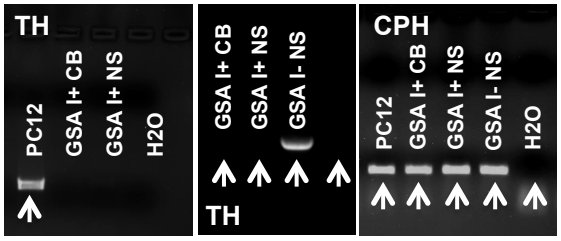

Related to Figure 4F

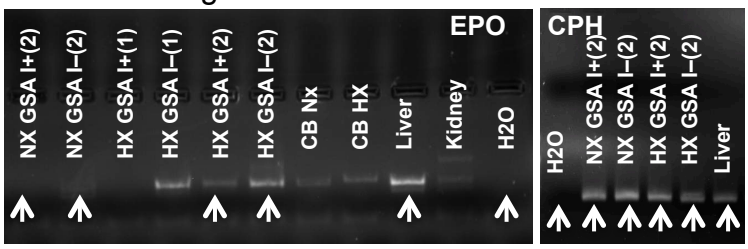

Related to Figure 4H

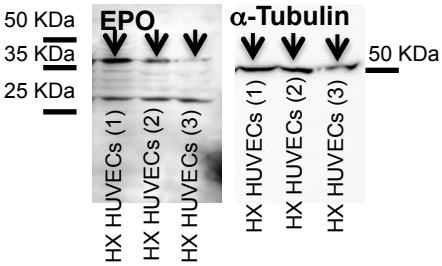

Related to Figure S3H

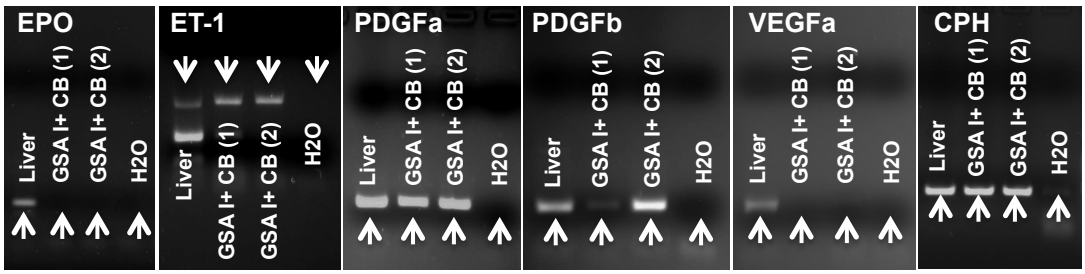

Related to Figure S3I

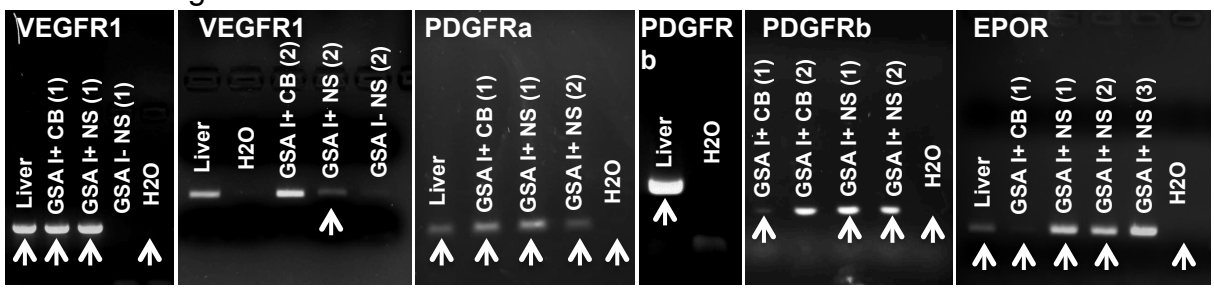

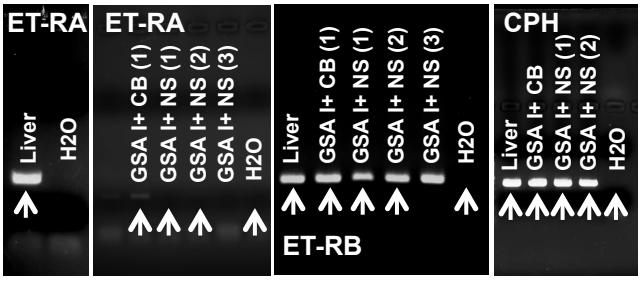

Related to Figure S3J

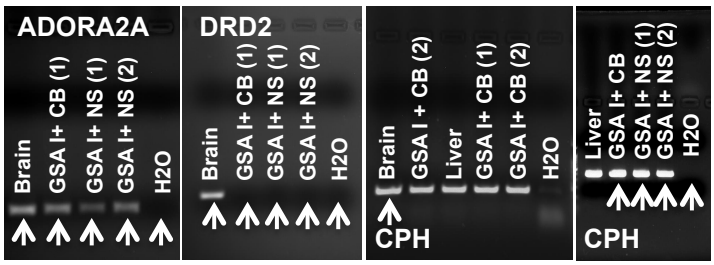

Figure S6. Original gels for PCRs and Western Blot, Related to Figures 3, 4, and S3.
Arrows point to the lanes used at the referred figures. All experiments and samples were run at the same time.

Table S1. Antibodies and reagents, Related to Experimental Procedures.

Name	Concentration	Use
Rb anti-TH, Novus Biological	1:1000	IHC, ICC
Chicken anti-β-galactosidase, Novus Biological	1:200	IHC
Rb anti-Tuj1, Abcam	1:500	ICC
Ms anti-smooth muscle actin (SMA), Sigma	1:500	ICC
Rb anti GFP, Invitrogen	1:500	ICC, IHC
Rb anti-GFAP, Dako	1:500	ICC
Ms anti-Nestin, Merck Millipore	1:500	ICC
Rb anti-GFP and YFP, Invitrogen	1:500	IHC
Ms anti-NG2 proteoglycan	1:500	ICC
Rb anti-Von Willembrand Factor, Sigma	1:200	ICC
Gt anti CD34, R&D	1:100	ICC, IHC
Gt anti-EPO, Santa Cruz	1:200	WB
PE-Rat anti-mouse CD31, BD	1:100	FC, ICC
Rb anti HIF-2a, Novus Biological	1:100	ICC
Alexa488-donkey-anti-rabbit IgG, Molecular Probes	1:1000	IHC, ICC
Alexa488-donkey-anti-mouse-IgG, Molecular Probes	1:1000	IHC, ICC
Alexa568-donkey-anti-Chicken IgG, Molecular Probes	1:1000	IHC, ICC
Alexa488-donkey-anti-Chicken, Molecular Probes	1:1000	ICC
Alexa568-donkey-anti-Goat IgG, Molecular Probes	1:1000	ICC
Rhodamine-Griffonia Simplicifolia lectin I, Vector Labs	1:100	IHC, ICC
FITC-Griffonia Simplicifolia lectin I, Vector Labs	1:100	IHC, ICC
5-bromo-3-indolyl-β-D-galactoside (bluo-gal), Invitrogen Life Technologies	2mM	EM
X-gal, Molecular Probes	2mM	ICC
DiI-labeled acetylated low density lipoproteins (DiI-AcLDL), Molecular Probes, Invitrogen	10 µg/ml	ICC
7-AAD, Molecular Probes	2 mg/ml	FC

IHC= Immunohistochemistry; ICC= Immunocytochemistry; EM= Electron Microscopy; FC= Flow Cytometry

Table S2. Sequences of oligonucleotides used as primers, Related to Experimental Procedures.

mRNA	sense	Sequence (5'→3')	Reference/Software
vWF	F R	CACTGCCCTCCAGGGAAAAT CGGATGCGCTTCTGAGAGAT	Primer Blast (NCBI)
eNOS	F R	GGATCCAGTGGGGGAAACTG TGGCTGAACGAAGATTGCCT	Primer Blast (NCBI)
VEGFa	F R	TTTTCGTCCAACTTCTGGGC TTCACCACTTCATGGGCTTTCT	Primer Blast (NCBI)
VEGFR1	F R	TTCCGGACTTTCAACACCTC CACCGAATAGCGAGCAGATT	Primer Blast (NCBI)
PDGFa	F R	GGAGCCATTCCCGCAGTTTG TCACCTCACATCCGTCTCCT	Primer Blast (NCBI)
PDGFb	F R	GCACCAATGCCAACTTCCTG GTTTGAGGTGTCTTGGCTCG	Primer Blast (NCBI)
PDGFRa	F R	TTCGCCAAGGTGGAAGAGAC ATCCCAAGATCCGACCAAGC	Primer Blast (NCBI)
PDGFRb	F R	GCGAAAACTGTCACCCACAC AGAGTGCGTCCCAGAACAAG	Primer Blast (NCBI)
EPO	F R	TACGTAGCCTCACTTCACTGCT CAGGTCACCTGTCCCCTCTC	Primer Blast (NCBI)
EPOR	F R	CGTCGAGTTTTGTGCCACTG GTCCAAGTCGCTAGCAGTCA	Primer Blast (NCBI)
ADORA2A	F R	GGCCGTGTGGATCAACAGTA AAGCCATTGTACCGGAGTGG	Primer Blast (NCBI)
DRD2	F R	CCAGTGAACAGGCGGAGAAT GTTTTGCCATTGGGCATGGT	Primer Blast (NCBI)
Enkephaline	F R	TACCTGCGCCATCTGAACAA TCTTGGCTAGCAAGTGGCTC	Primer Blast (NCBI)
ET-1	F R	ATCATCTGGGTCAACACTC GAATCTCCTGGCTCTCTG	(Kugelmeier et al., 2008)
ET_A	F R	TTCGTCATGGTACCCTTCGA GATACTCGTTCCATTCATGG	(Kugelmeier et al., 2008)
ET_B	F R	TTCACCTCAGCAGGATTCTG AGGTGTGGAAAGTTAGAACG	(Kugelmeier et al., 2008)
Cdh5	F R	GCACAGGCGGGTGTCAGCAT TCTCTCTGGGCCCTCCGTGC	Primer Blast (NCBI)
TH	F R	GGACATTGGACTTGCATCTCTGGG TGAGAAGCAGTGTTGGGAGGATGG	Primer Express
EPAS1 Q	F R	GCAGATGGATAACTTGTACCTGAAAG CTGACAGAAGATCATATCACCGTCTT	Primer Blast (NCBI)
GLUT1 Q	F R	CCCGCTTCCTGCTCATCAA GACCTTCTTCTCCCGCATCA	Primer Blast (NCBI)
VEGFa Q	F R	CGCAAGAAATCCCGGTTTAA CAAATGCTTTCTCCGCTCTGA	Primer Blast (NCBI)

F, forward; R, reverse; Q, control.

Supplemental Experimental Procedures

***In Vivo* Hypoxic Treatments and Drug administration**

Transgenic mice (4-6 weeks old or 8-9 months old for DMOG *in vivo* experiments) and rats (6 weeks old) were chronically exposed to a 10% O2 environment during 7 days by using a specially designed hermetic isobaric chamber, with O2 and CO2 controls, and temperature and humidity monitoring (Coy Laboratory Products, Inc.; Grass Lake, MI, USA). A correct hypoxic stimulus was confirmed by measuring hematocrit (Figure 4K and S5C). Age-matched control mice and rats were similarly housed in ambient air outside the chamber. *GFAP-cre/floxed LacZ* or YFP mice used for cell fate mapping were always exposed twice to hypoxia. The first exposure was 7 days long and allowed the activation of the hGFAP-cre construct during the subsequent re-normoxia (14 days long; see Pardal et al., 2007 and Figure S1). For *in vivo* experiments with Tyrphostin AG490, *GFAP-cre/floxed LacZ* mice were injected with AG490 one day before the beginning of the hypoxic period and then three times per week during the exposition to the hypoxic environment (266,7 μg/mouse). Tyrphostin AG490 (5mg; Calbiochem, Millipore) was dissolved in 1 mL of sterile DMSO and brought to a final concentration of 2.2 mM by diluting in sterile PBS 1X. Control mice were injected with equal volume of the vehicle. Each group included the analysis of 3 cell suspensions, each obtained from 2 mice (4 CBs). Animals were maintained in the hypoxic environment for 7 days. For *in vivo* experiments with dimethyloxalylglycine (DMOG, Frontier Scientific), normoxic *GFAP-cre/floxed YFP* mice were injected with DMOG intraperitoneally twice per day at a dose of 80 mg/Kg during 12 days. When preparing a 200 mg/mL stock solution of DMOG, the compound was dissolved in DMSO. Fresh working solution was prepared every day, diluting the stock solution to a final concentration of 20 mg/mL in saline and storing it at 4ºC in dark for a maximum of 24 h. Normoxic control mice were injected twice daily with vehicle at the same time. In the hypoxic experimental group, animals were exposed during 12 days to chronic hypoxia. Each group included 6-8 mice in order to obtain 3 CB cell dispersions from 2-3 mice each. Mice were housed in standard rodent cages with 24 h access to pellet food and water.

Dissociation of Carotid Body Cells

Rat and transgenic mouse CBs were dissociated by enzymatic treatment in PBS solution containing 0.6 mg/ml collagenase type II (Sigma), and 0.3 mg/ml trypsin (Sigma), for 20 min at 37°C in a crystal flask at 600 rpm in a Thermomixer Comfort (eppendorf). After enzymatic treatment, 2 volumes of staining solution were added to quench enzymes. Staining solution contained (for 50 ml): 44 ml L15 medium (GIBCO), 0.5 ml penicillin/streptomycin (GIBCO), 0.5 ml 1 M HEPES buffer (GIBCO), 0.1 g BSA (Sigma), and 5 ml distilled and deionized water. Dissociated CB cells were centrifuged for 5 min at 300 g at 4ºC. Afterwards, the cell pellet was resuspended and the cells were plated on an ultralow binding well for neurosphere assays, or used for immunocytochemistry.

Transfection of Carotid Body or Neurosphere Cells

Rat CBs were dissociated by enzymatic treatment following the protocol described above. Dissociated cells were plated on ultralow binding wells and transfected with lipofectamine 2000 following vendor instructions (Invitrogen, Life Technologies). For transfection, 2.5 μg of pGFAP-eGFP plasmid was used. After 36h in culture, transfected cells were resuspended and sorted by flow cytometry.

EPAS1 (HIF-2α) siRNA experiments were carried out using predesigned SmartPool siRNA (Dharmacon). Neurospheres were dissociated with sequential incubation at 37ºC during 10 minutes in papain (28.1 Units per mg of protein, Worthington) at a final concentration of 35 μL/mL in HBSS, and in 0.6 mg/ml collagenase type II (Sigma) at a final concentration of 66 μL/mL in HBSS. NS cells were cultured onto adherent, using 5 μg/mL fibronectin (Biomedical technologies Inc.) to pre-treat the 24-well plates, and with complete neural crest medium, overnight. Initially, to optimize transfection efficiency, EPAS1 knock-down was analyzed by Real Time quantitative PCR, with cells transfected using 25 nM, 50 nM or 100 nM siRNA, complexed to 2 μL of lipofectamine 2000 reagent, following manufacturer instructions (Invitrogen, Life Technologies). EC differentiation assays were performed transfecting NS cells with 50 nM siRNA. After transfection (12-18h later), cells were exposed to hypoxia (3% O2) for 24h if used for RNA extraction, or for 72h if used for EC differentiation functional assay. Control cells were transfected with the same amount of control siRNA smart pool (Dharmacon).

Neurosphere Assays

Dispersed rat CB cells were typically cultured in ultralow binding 6-well plates (Corning Inc., Corning, NY) at a clonal density of 10,000 cells per well, so that individual neurospheres were spatially apart from each other. Culture medium contained D-MEM:F-12 (GIBCO BRL, Grand Island, NY) with 15% FBS

(GIBCO), 1% N2 supplement (GIBCO), 2% B27 supplement (GIBCO), 1% penicillin/streptomycin (GIBCO), 20 ng/ml recombinant human bFGF (R&D Systems, Minneapolis, MN), 20 ng/ml recombinant human IGF-1 (R&D Systems), and 20 ng/ml recombinant human EGF (R&D Systems). All cultures were maintained in O2 and CO2-controlled incubators (Thermo Electron Corp., Waltham, MA) at 21% or 3% O2 and 37ºC. Cell cultures exposed to hypoxia were tested for the expression of typical hypoxia-responsive genes to confirm a correct stimulus (Figure 3C and D).

Endothelial Differentiation Assay

To study the induction of endothelial differentiation in adherent NS cultures we exposed cells to different factors: 7 IU/mL erythropoietin (EPO, Binocrit®), 0.1 μM endothelin-1 (ET-1, Sigma), 25 ng/mL platelet-derived growth factor (PDGF, R&D), 25 ng/mL vascular endothelial growth factor (VEGF, R&D), 100 μM adenosine (ADO, Sigma), 10 μM dopamine (DA, Sigma) and 10 μM met-encephalin (Met-enk, Sigma), or 3% hypoxia. Factors were added every day to standard culture medium without mitogens. For EPO pathway inhibition, EPO (7IU/ml) was added to low serum concentration medium (5% FBS, GIBCO) without mitogens and supplemented, where necessary, with EPO-neutralizing antibody (1:20) (Santa Cruz) or 50 μM Tyrphostin AG490 (Calbiochem). Inhibition of prolyl-hydroxylases during EC differentiation in hypoxic adherent NS cultures was achieved by adding DMOG (Frontier Scientific) daily, dissolved in DMSO, to a final concentration of 0.1 mM or 1 mM. Controls were performed adding the same volume of vehicle.

Immunocytochemistry

Adherent cultures: Adherent neurosphere colonies were fixed in 4% PFA, pre- blocked for at least 1h at room temperature, and incubated with the primary and secondary antibodies for 1h each, at RT. The blocking solution was the same than for tissues (see above). Details about the antibodies used are given in Table S1. Incubation in 1:100 Rhodamine or Fluorescein- conjugated GSA I in PBS during 1 hour at RT was performed prior to DAPI counter-staining.

Cells in suspension: Dispersed CB cells were collected in conical tube, fixed in 4% PFA (prepared in PBS) for 10 min at RT and washed in PBS by centrifuging at 300g 5 minutes at 4ºC. Both primary and secondary antibody immunoreaction or Rhodamine conjugated GSA I staining was carried out in PBS with calcium an magnesium plus 10% FBS 1h at RT. Finally, nuclei were counterstained by DAPI. Cells were pulled down on poly-lysin coated slides (Thermo scientific) by centrifuging at 1000 rpm 5 minutes in Shandon Cytospin 4 (Thermo Electron Corporation). Details about the antibodies used are given in Table S1.

Fluorescent immunohistochemistry

Following normoxic/hypoxic treatments, animals were anaesthetized with ketamine (100 mg/kg) plus xylazine (10 mg/kg), intracardially perfused with 4% PFA (Sigma), and the carotid bifurcations dissected and postfixed in PFA for 2 hr. After overnight cryoprotection in 30% sucrose solution (Sigma), bifurcations were embedded in OCT compound (Sakura Finetek) and frozen in dry ice. Sections (10 μm thick) of the carotid body within the carotid bifurcation were cut on a Leica cryostat. For immunohistochemistry we used the standard staining procedure previously published (Pardal et al., 2007). Antibodies used are listed in Table S1. Fluorescent specimens were viewed under a confocal microscope with a 63x immersion-oil objective. Image J software (National Institute of Health, USA) was used for cell number quantifications. In the case of anti-β-Gal antibody, we were only able to analyze 2 normoxic and 2 hypoxic animals due to this antibody running out of production.

For detection of endothelial cells in histological studies we used Griffonia Simplicifolia lectin I (GSA I; Vector Labs) (Laitinen, 1987; Bankston et al., 1991). After antibody immunostainings, sections were incubated in GSA I lectin, diluted 1:100 in PBS, for 1h at room temperature. Finally, slides were counter stained with 2.5 mg/ml DAPI (Sigma) for 15 min at room temperature, and then mounted using Fluorogel mounting medium (Electron Microscopy Sciences).

DAB immunohistochemistry

Endogenous peroxidases were inhibited by incubating tissue sections in 0.3% H2O2 and 10% Methanol in PBS, pH 7.4, for 20 minutes at RT. Non-specific antibody binding sites were blocked by incubating in 10% Normal Horse Serum (NHS, GIBCO), 0.3% Triton X-100 in 0.1 M PBS, pH 7.4, for 2 hours at RT. Slices were successively incubated overnight at 4ºC with specific anti-GFP primary antibody (see Table S1) diluted in 1% NHS, 0.3% Triton X-100, followed by an incubation with biotynilated Goat anti-rabbit IgG secondary antibody (Vector Labs), diluted 1:1000 in the same diluent used for primary antibody, for 1 hour. Sections were incubated in avidin-biotin-peroxidase complex, diluted 1:100 (ABC kit, Vectastain Elite, Vector Labs), for 30 minutes at RT. Antibody binding sites were revealed incubating sections in

3,3'- diaminobenzidine (DAB; Peroxidase (HRP) Kit, Vector Labs) for 1 minute. Negative controls were obtained by omitting primary antibody. Sections were counterstained with hematoxylin and coverslipped using Eukitt mounting medium (Electron Microscopy Sciences, EMS), after dehydration in a series of ethyl alcohols and xylene.

Electron microscopy

Following normoxic/hypoxic treatments, animals were anaesthetized with ketamine (100 mg/kg) plus xylazine (10 mg/kg) and intracardially perfused with PBS-based 4% PFA (Sigma). Carotid bifurcations were dissected and postfixed in the same fixative for 2 hours. Bluo-gal staining: *GFAP-Cre/floxed LacZ* and *Wnt1-Cre/floxed LacZ* CB 50 μm thick sections were fixed in 4% PFA in PBS pH 7.4, rinsed twice in PBS, and stained in 2 mM 5-bromo-3-indolyl-β-D-galactoside (bluo-gal; Invitrogen Life Technologies) in PBS. Bluo-gal was dissolved in PBS containing 20 mM potassium ferrocyanide, 20 mM potassium ferricyanide, 2 mM MgCl2 and 0.3% Triton-X, as previously described (Weis et al., 1991; Joseph et al., 2004). The staining was performed for 24 hours at 37°C. Sections were removed from the bluo-gal buffer, rinsed in PBS, then postfixed in 2.5% glutaraldehyde overnight at 4°C in agitation. CB sections were then rinsed in 0.1 M PB pH 7.4 and postfixed in aqueous 1% OsO4 for 1h at RT. Sections were rinsed in PB then dehydrated in an ethanol series (30, 50, 70, 80, 95 and 100% ethanol) before infiltrating and embedding in Spurr resin (Bozzola and Russell, 1992). Semithin sections (1 μm thick) were cut with a glass knife. Ultrathin sections (60 nm) were cut with a diamond knife and examined without further staining to facilitate visualization of the bluo-gal precipitates. Note that the presence of Triton-X detergent in the bluo-gal buffer resulted in poor preservation of membranes. However, Triton-X was required for effective bluo-gal staining.

Image acquisition and processing

Immunofluorescent images: Microscope: Olympus BX61; Type/ magnification/ numerical aperture of objectives: UPlanFl/20x/0.50, UPlanFl/40x/0.75, UPlanFl/100x/1.30 with oil immersion; Temperature: RT; Imaging medium: Fluoro-Gel (Electron Microscopy Science); Fluorochromes: Alexafluor 568, Alexafluor 488; Camera: Olympys DP70; Acquisition software: DP Controller; Post-acquisition processing: Photoshop (contrast control by 'Level' tool).

Bright field images: Microscope: Olympus BX 61; Type/ magnification/ numerical aperture of objectives: UPlanFl/20x/0.50, UPlanFl/40x/0.75; Temperature: RT; Imaging medium: Eukitt (Electron Microscopy Sciences); Camera: Olympus DP70; Acquisition software: DP Controller; Post-acquisition processing: Photoshop: (brightness/contrast adjustment).

Confocal images:

- Microscope: Zeiss LSM 7 DUO; Type/ magnification/ numerical aperture of objectives: Plan Apochromat/63x/1.40 with oil; Acquisition software: Zeiss Zen2011; Post-acquisition processing: Zeiss Zen2011 Lite (maximum projection and orthogonal view).
- Microscope: Nikon Nikon Eclipse Ti-E; Type/ magnification/ numerical aperture of objectives: Plan Apo/60x/1.40 with oil; Acquisition software: Nikon NIS-Elements C; Post-acquisition processing: Nikon NIS-Elements C (maximum projection and orthogonal view).

All the acquisitions were carried out at room temperature. Imaging medium: Fluoro-Gel (Electron Microscopy Sciences).

Electron microscopy images: Microscope: Philips CM-10; Temperature: RT; Acquisition software: iTEM solution SIS (Olympus); Camera: Veleta (Olympus); Post-acquisition processing: Photoshop (brightness/contrast adjustment).

Flow Cytometry

After incubation at 37ºC, in ultralow binding wells over night for the antigen retrieval, cells obtained from enzymatic digestion of mouse CBs were resuspended in a volume of 100 μL and were incubated for 1 hour in the dark at 4 ºC with PE-conjugated monoclonal antibodies against mouse CD31 (BD Biosciences, 1:100). For separating and analyzing GSA I+ cells from the different samples (CBs, NS, or adherent NS), we used a protocol modified from (Sahagun et al., 1989). In the case of flat NS colonies, obtained by culturing NS on fibronectin and in the presence of EPO during 5 days, cells were removed from the petri dish by treating with 0.25% trypsin + 0.1% EDTA for 5 minutes at 37ºC. Both CB and NS dissociated cells were re-seeded in ultralow binding wells and incubated at 37ºC in complete medium without mitogens overnight. Cells were then pelleted and resuspended in PBS with Calcium and Magnesium supplemented with 10% FCS. FITC-GSA I was added to a final dilution of 1:100, and cells were incubated on ice for 30 minutes. As controls, some tubes received either no lectin or lectin preincubated with 0.2M galactose. After washing off unbound molecules, cells were resuspended in

staining medium containing 2 mg/ml 7-AAD (Molecular Probes). Dead cells were eliminated from sorts and analyses as 7-AAD+.

Reverse Transcriptase-Polymerase Chain Reaction and Real Time quantitative PCR
Total RNA was extracted from GSA I positive and negative cell fractions, sorted from dispersed adherent NS or dispersed rat CBs, using a commercial kit (RNeasy MICRO kit; Qiagen), following manufacturer instructions. In the case of NS, cells were separated after induced endothelial differentiation during 5 days by EPO treatment (see above). For the RNA extraction, 8-10 x 10^4 cells were used. Rat brain, liver, kidney and PC12 cell line were used as positive expression controls and were processed for total RNA extraction using Trizol reagent (Invitrogen), following the protocol recommended by the manufacturer. For retrotranscription, cDNA was synthesized with QuantiTec Reverse transcription kit (Qiagen), as indicated by manufacturer instructions. Standard PCR was performed with 20 ng of first strand cDNA. Loading control used was cyclophilin (CPH). Real-time quantitative PCR was performed in an ABI Prism 7500 Sequence Detection System using the thermocycler conditions recommended by the manufacturer (Applied-Biosystems). Detection was performed with SYBR Green PCR Master Mix.

Western blot
Preparation of cell protein extracts: HUVECs (10^6 cells) were exposed for 3 days to a hypoxic environment (3% O2). For preparing whole cell protein extracts, cells were washed once with ice-cold PBS (GIBCO) and lysed with 500 μL of lysis buffer (150 mM NaCl, 10 mM Tris pH 7.9, 1 mM EDTA, 1% SDS, 1% Triton X-100 and 1X protease inhibitor cocktail (Roche)) for 20 minutes on ice. The lysates were centrifuged at 15000 X g for 30 minutes at 4ºC and supernatants containing proteins were collected and stored at -20 ºC. Protein concentration of supernatants were quantified using a protein Bradford assay reagent (Sigma). Aliquots of the supernatants were mixed with 4X reducing loading buffer, boiled for 3 minutes and stored at -20ºC until use.
Electrophoresis and immunoblotting: 80 μg of total cell lysate per lane was subjected to 12% SDS-PAGE and transferred onto PVDF membrane (0.45 pore size; Millipore). The efficiency of loading transfer was confirmed by staining the PVDF membrane with Ponceau S (Sigma-Aldrich). Filters were blocked 2 hours at RT with 5% nonfat dry milk powder in TBS-T (10 mM Tris pH 7.5, 100 mM NaCl, and 0.05% Tween 20). Membranes were washed in TBS-T and incubated with a Goat polyclonal anti EPO antibody (Santa Cruz) over night at 4ºC with gentle shacking. α-Tubulin (Sigma-Aldrich) served as loading and transfer control. After washing with TBS-T, HRP- conjugated anti-Goat IgG antibody (Biomedal) was added. Immunoreactive proteins were revealed using an enhanced chemiluminescence (ECL) kit (GE Healtcare).

Statistics
Sample size was chosen based on previous results or pilot studies. In any case, we expected to obtain a moderate-to-large effect size to ensure a power of 0.8, and an alpha of 0.05. Additionally, we took into account technical difficulties that could affect the good quality of the samples. Hence, we opted to increase the sample size up to 20% of the initial sample size estimation. In all cases we tried to respect the principles of 3Rs (Replacement, Reduction and Refinement). The experiments were pseudo-randomized with regards to sex (in order to guarantee a 50% of males and females in the different animal groups) and completely randomized with regards to allocation to different experimental groups. The investigator was completely blinded when assessing the outcome. Data are always presented as the mean ± standard error of the mean (s.e.m.), and the number of experiments carried out with independent cultures/animals (n) is shown in figure legends.

Supplemental References

Arsenault, P.R., Pei, F., Lee, R., Kerestes, H., Percy, M.J., Keith, B., Simon, M.C., Lappin, T.R., Khurana, T.S., and Lee, F.S. (2013). A knock-in mouse model of human PHD2 gene-associated erythrocytosis establishes a haploinsufficiency mechanism. The Journal of biological chemistry *288*, 33571-33584.

Bankston, P.W., Porter, G.A., Milici, A.J., and Palade, G.E. (1991). Differential and specific labeling of epithelial and vascular endothelial cells of the rat lung by Lycopersicon esculentum and Griffonia simplicifolia I lectins. European journal of cell biology *54*, 187-195.

Barriga, E.H., Maxwell, P.H., Reyes, A.E., and Mayor, R. (2013). The hypoxia factor Hif-1alpha controls neural crest chemotaxis and epithelial to mesenchymal transition. The Journal of cell biology *201*, 759-776.

Benelli, R., and Albini, A. (1999). In vitro models of angiogenesis: the use of Matrigel. The International journal of biological markers *14*, 243-246.

Bishop, T., Talbot, N.P., Turner, P.J., Nicholls, L.G., Pascual, A., Hodson, E.J., Douglas, G., Fielding, J.W., Smith, T.G., Demetriades, M*., et al.* (2013). Carotid body hyperplasia and enhanced ventilatory responses to hypoxia in mice with heterozygous deficiency of PHD2. The Journal of physiology *591*, 3565-3577.

Bozzola, J.J., and Russell, L.D. (1992). Electron microscopy: principles and techniques for biologists (Boston, MA, Jones & Bartlett Publishers).

Hodson, E.J., Nicholls, L.G., Turner, P.J., Llyr, R., Fielding, J.W., Douglas, G., Ratnayaka, I., Robbins, P.A., Pugh, C.W., Buckler, K.J*., et al.* (2016). Regulation of ventilatory sensitivity and carotid body proliferation in hypoxia by the PHD2/HIF-2 pathway. J Physiol *594*, 1179-1195.

Joseph, N.M., Mukouyama, Y.S., Mosher, J.T., Jaegle, M., Crone, S.A., Dormand, E.L., Lee, K.F., Meijer, D., Anderson, D.J., and Morrison, S.J. (2004). Neural crest stem cells undergo multilineage differentiation in developing peripheral nerves to generate endoneurial fibroblasts in addition to Schwann cells. Development *131*, 5599-5612.

Kaelin, W.G., Jr., and Ratcliffe, P.J. (2008). Oxygen sensing by metazoans: the central role of the HIF hydroxylase pathway. Molecular cell *30*, 393-402.

Kugelmeier, P., Nett, P.C., Zullig, R., Lehmann, R., Weber, M., and Moritz, W. (2008). Expression and hypoxic regulation of the endothelin system in endocrine cells of human and rat pancreatic islets. JOP : Journal of the pancreas *9*, 133-149.

Laitinen, L. (1987). Griffonia simplicifolia lectins bind specifically to endothelial cells and some epithelial cells in mouse tissues. The Histochemical journal *19*, 225-234.

Melero-Martin, J.M., Khan, Z.A., Picard, A., Wu, X., Paruchuri, S., and Bischoff, J. (2007). In vivo vasculogenic potential of human blood-derived endothelial progenitor cells. Blood *109*, 4761-4768.

Pardal, R., Ortega-Saenz, P., Duran, R., and Lopez-Barneo, J. (2007). Glia-like Stem Cells Sustain Physiologic Neurogenesis in the Adult Mammalian Carotid Body. Cell *131*, 364-377.

Platero-Luengo, A., Gonzalez-Granero, S., Duran, R., Diaz-Castro, B., Piruat, J.I., Garcia-Verdugo, J.M., Pardal, R., and Lopez-Barneo, J. (2014). An o2-sensitive glomus cell-stem cell synapse induces carotid body growth in chronic hypoxia. Cell *156*, 291-303.

Sahagun, G., Moore, S.A., Fabry, Z., Schelper, R.L., and Hart, M.N. (1989). Purification of murine endothelial cell cultures by flow cytometry using fluorescein-labeled griffonia simplicifolia agglutinin. The American journal of pathology *134*, 1227-1232.

Weis, J., Fine, S.M., David, C., Savarirayan, S., and Sanes, J.R. (1991). Integration site-dependent expression of a transgene reveals specialized features of cells associated with neuromuscular junctions. The Journal of cell biology *113*, 1385-1397.